

Accepted by AJ, July 11, 2005

The FIRST-Optical-VLA Survey for Lensed Radio Lobes

Deborah B. Haarsma¹, Joshua N. Winn^{2,3}, Emilio E. Falco⁴, Christopher S. Kochanek⁵, Philip Ammar¹, Catherine Boersma¹, Shannon Fogwell¹, T. W. B. Muxlow⁶, Brian A. McLeod², Joseph Lehar^{2,7}

ABSTRACT

We present results from a survey for gravitationally lensed radio lobes. Lensed lobes are a potentially richer source of information about galaxy mass distributions than lensed point sources, which have been the exclusive focus of other recent surveys. Our approach is to identify radio lobes in the FIRST catalog and then search optical catalogs for coincident foreground galaxies, which are candidate lensing galaxies. We then obtain higher-resolution images of these targets at both optical and radio wavelengths, and obtain optical spectra for the most promising candidates. We present maps of several radio lobes that are nearly coincident with galaxies. We have not found any new and unambiguous cases of gravitational lensing. One radio lobe in particular, FOV J0743+1553, has two hot spots that could be multiple images produced by a $z = 0.19$ spiral galaxy, but the lensing interpretation is problematic.

Subject headings: gravitational lensing — galaxies: individual (FOV J0743+1553) — galaxies: spiral — radio continuum: galaxies

1. Introduction

Gravitational lenses are prized for their ability to tell us about galaxies. The configuration of the multiple images of an extragalactic background source provides a direct and accurate measurement of the enclosed mass of the foreground galaxy, including the contribution due to dark matter

¹Calvin College, 1734 Knollcrest SE, Grand Rapids, MI 49546, dhaarsma@calvin.edu

²Harvard-Smithsonian Center for Astrophysics, 60 Garden Street, Cambridge, MA 02138

³Hubble Fellow

⁴F.L. Whipple Observatory, Smithsonian Institution, P.O. Box 97, Amado, AZ 85645

⁵Department of Astronomy, The Ohio State University, 4055 McPherson Lab, 140 West 18th Avenue, Columbus, OH 43210

⁶University of Manchester, Jodrell Bank Observatory, Macclesfield, Cheshire SK11 9DL, UK

⁷Current address: CombinatoRx, Inc., 650 Albany St., Boston, MA 02118, and Boston University Bioinformatics, 44 Cummington St., Boston, MA 02115

(as reviewed by Narayan & Bartelmann 1999; Courbin, Saha, & Schechter 2002; Kochanek et al. 2004). Lenses can be used to study the mass distributions of individual galaxies (Kochanek 1991; for recent examples see Trotter, Winn, & Hewitt 2000; Cohn et al. 2001; Rusin et al. 2002), as well as statistical properties of galaxy mass distributions such as the degree of alignment of mass and light (e.g., Keeton, Kochanek, & Seljak 1997), the radial mass distribution (e.g., Davis, Huterer, & Krauss 2003; Rusin, Kochanek, & Keeton 2003b), and the degree of central concentration (Rusin & Ma 2001). One the most successful applications of lenses has been to measure the evolution of the mass-to-light ratio of field galaxies with cosmic epoch (Kochanek et al. 2000b; Chae & Mao 2003; Rusin et al. 2003a; van de Ven, van Dokkum, & Franx 2003; Ofek, Rix, & Maoz 2003).

Our ability to use lenses in this manner is limited by the relatively small number of known lenses and the small number of constraints that each one imposes on the mass distribution (see Kochanek et al. 2004). We have undertaken a survey (which we term the FIRST¹-Optical-VLA², or FOV, survey), the goal of which is not only to discover more lenses, but to discover lenses in which the background source is extended rather than pointlike. For the purpose of studying the mass distribution of the foreground galaxy, gravitationally lensed extended structures provide a potentially richer set of constraints than lensed point sources.

Many of the approximately 90 known cases of multiple-image lensing by galaxies were discovered in systematic lens surveys. Of these, roughly equal numbers were discovered by imaging surveys of radio sources [e.g. MG-VLA (Burke et al. 1993), JVAS/CLASS (Browne et al. 2003), and PMN-NVSS (Winn 2001; Winn et al. 2002b)] and optically selected quasars [HST snapshot surveys (Maoz et al. 1993; Gregg et al. 2000) and ground based surveys such as WFI (Morgan et al. 2004), the Hamburg-ESO survey (Wisotzki et al. 2004), and the SDSS³ (Oguri et al. 2005)]. Optical surveys have generally resulted in a larger number of lenses per source examined, because of a greater magnification bias (the tendency for lensed quasars to be over-represented in a flux-limited sample) than radio-selected samples. On the other hand, radio surveys have the advantages of the superior angular resolution and high degree of automation of the VLA, and freedom from extinction by dust. Radio surveys also differ from optical surveys in that the background sources are not necessarily point sources, as are optically-selected quasars. The classical “double-lobed radio galaxy” has a compact core of radio emission near the center of the galaxy, and thin jets of radio emission leading to more diffuse lobes that can be located hundreds of kiloparsecs away. The relative intensities of the core, jet, and lobe components varies considerably from one source

¹Faint Images of the Radio Sky at Twenty-Centimeters, <http://sundog.stsci.edu>

²The Very Large Array (VLA) is operated by the National Radio Astronomy Observatory (NRAO), a facility of the National Science Foundation operated under cooperative agreement by Associated Universities for Research in Astronomy (AURA), Inc.

³Funding for the Sloan Digital Sky Survey (SDSS) has been provided by the Alfred P. Sloan Foundation, the Participating Institutions, the National Aeronautics and Space Administration, the National Science Foundation, the U.S. Department of Energy, the Japanese Monbukagakusho, and the Max Planck Society. The SDSS Web site is <http://www.sdss.org>.

to another, and also with observing frequency.

The largest and most recent radio surveys (JVAS/CLASS and PMN–NVSS) concentrated on finding lensed radio cores, rather than lobes. The cores are typically point-like at arcsecond resolution, and can be selected from catalogs with poorer resolution by virtue of their flat radio spectra, whereas lobes are typically diffuse and have steep radio spectra⁴. These surveys have been very successful, finding about one lens per 700 targets imaged by the VLA. There are several reasons why flat-spectrum sources were preferred. First, the simple structure of the cores makes lenses relatively easy to recognize: they have multiple compact components separated by $\sim 1''$. Second, the high surface brightness of cores facilitates the interferometric imaging process (i.e., self calibration and deconvolution). Third, the radio cores or their optical counterparts sometimes have time-variable fluxes, allowing the determination of time delays and thus a combination of the Hubble constant and the surface density of the lens (see, e.g., Kochanek 2003). Fourth, the measured lensing probability, which can be used to estimate the cosmological model (Turner 1990; Fukugita et al. 1992), is easier to interpret in a survey of point sources than a survey of extended structures.

The main disadvantage of flat spectrum surveys, as already mentioned, is that lensed point sources do not supply many constraints on the mass distribution of the lens galaxy. The simple two-image and four-image lenses that are the primary yield of the flat spectrum surveys provide estimates of the mass and the mean quadrupole of the lens galaxy, but little else. Furthermore, the flat-spectrum surveys have already examined most of the sources in the sky that are sufficiently bright to be observable with the very short VLA observations (about 30 seconds) that are necessary to make up for the low lensing probability. This situation will change with the development of the EVLA⁵ and e-MERLIN⁶, but these capabilities are still some years away.

Our survey pursues the population of extended radio sources: jets and lobes that are lensed into partial or complete Einstein rings. In fact, these steep-spectrum lenses outnumber the flat-spectrum lenses on the sky. Flat and steep spectrum sources are similar in number density and redshift distribution, but the greater angular extent of the steep spectrum sources greatly enhances the probability that a foreground galaxy is close enough to the line of sight for strong lensing to occur (Kochanek & Lawrence 1990). We expect roughly 75% of radio lenses to be steep spectrum sources. Indeed, many of the lenses found by the MG–VLA image survey, which targeted both flat and steep spectrum radio sources, were Einstein rings: MG 1131+0456, (Hewitt et al. 1988), MG 1654+1346 (Langston et al. 1989), MG 1549+3047 (Lehár et al. 1993), and MG 0751+2716 (Lehár et al. 1997). The Einstein rings PKS 1830-211 (Jauncey et al. 1991) and B 0218+357 (Patnaik et al. 1993) were

⁴Here, “flat” means that the radio flux density is a weak function of observing frequency, and “steep” means that the flux density declines sharply with frequency. Supposing $S_\nu \propto \nu^{-\alpha}$, the cutoff between flat and steep is often taken to be $\alpha \approx 0.5$.

⁵Expanded Very Large Array (ELVA) <http://www.aoc.nrao.edu/evla>

⁶e-MERLIN <http://www.merlin.ac.uk/e-merlin>

found in flat spectrum surveys, although the rings in these systems are much fainter than the cores. The challenge of steep-spectrum surveys, as discovered by the MG–VLA survey, is that the complex structure of the radio sources means that more follow-up observations are required to separate the lenses from unlensed lobes that happen to have intrinsically ring-like morphology. Nonetheless, it is worth finding the steep spectrum lenses—many applications of lenses are still limited by the available numbers of systems, and the extended structure of the steep spectrum lenses provide far more constraints on mass distributions.

We have developed a more efficient method to find steep-spectrum lenses (Lehár et al. 2001). Rather than starting with a complete catalog of radio sources (as the MG–VLA survey), we pre-select sources that are likely to be radio lobes, by employing a source catalog with sufficiently good angular resolution. Then we search for optical objects at the same position as the lobes. Because radio lobes themselves have no optical emission, any galaxy that is detected is likely to be a foreground galaxy, and therefore a potential lens galaxy. In particular, we combine the relatively high resolution FIRST survey with relatively deep optical surveys (APM⁷ and SDSS). This strategy proved successful in our pilot study (Lehár et al. 2001) where we used this method on a portion of the FIRST catalog, finding 2 lenses (the new lens FOV J0816+5003, and a re-discovery of MG 1549+3047) among a list of only 33 candidates.

Here we describe an extension of the FOV survey to a larger portion of the FIRST catalog. In §2 we describe the selection of targets from radio and optical catalogs. In §3 and §4 we present follow-up radio and optical observations of these targets, which greatly narrowed the list of lens candidates. In §5 we describe the particular candidate FOV J0743+1553 in some detail, since the initial observations appeared to be promising. We discuss the other candidates in §6, and summarize our conclusions in the final section. In this paper, we assume a flat, $\Omega_m = 0.3$ cosmology with $h = 0.72$ whenever cosmological calculations are needed.

2. Target Selection

The target selection process had four steps: selection of a flux-limited sample of radio sources; identification of likely radio lobes; identification of any optical counterparts to the lobes; and final visual inspection to filter out catalog errors and prioritize candidates for further follow-up. In this section we describe each of these steps in more detail.

The flux-limited sample was drawn from the VLA FIRST catalog of radio sources (Becker, White, & Helfand 1995). This 20 cm (1.4 GHz) survey is complete to ~ 1 mJy, with a beam size of $5''.4$ FWHM. While the angular resolution is not fine enough to detect the arcsecond-scale separations between lensed images, it does suffice to identify objects that are likely to be radio

⁷Cambridge Automated Plate Measurement (APM) of POSS-1 and UKST plates
<http://www.ast.cam.ac.uk/~apmcat>

lobes. For our survey we consulted the 2001 October 15 edition of the catalog, which contained 771,076 radio objects in 7954 square degrees in the north Galactic cap and 611 square degrees in the south Galactic cap. We selected objects brighter than 3 mJy that were not flagged as radio sidelobes (375,919 objects).

Next, we identified likely radio lobes. Following the algorithm presented in the appendix of Lehar et al. (2001), we identified groups of two or more FIRST sources that were spaced closely enough to represent the core and lobe (or lobes) of a single radio galaxy. In particular we selected groups in which the maximum separation between any two sources is less than $90''$, and in which no two sources are separated by more than $60''$ (these numbers were chosen with reference to the typical size of radio galaxies). For groups with three or more sources, the algorithm selected those that are more symmetric (symmetry factor $S > 0.50$) and less bent (bending angle $\theta < 30^\circ$) (see the appendix of Lehar et al. 2001 for definitions of S and θ). The algorithm then identified which components in the group are likely to be lobes and which component is likely to be the core (using the extent of the objects and their location within the group). Of these groups, we selected those which would be most readily observable: we required that at least one object in the group be bright enough for self-calibration (>10 mJy at 20 cm), and that the lobes be small enough to provide sufficient contrast in high-resolution follow-up observations ($<10''$). This gave us 30,927 radio galaxies with identifiable, bright lobes.

To find optical objects at the same position as the radio lobes, we used the Cambridge APM scans of the POSS-I and UKST plates. The POSS-I plates cover the northern sky to a limiting magnitude of 21.5 in O (blue) and 20 in E (red). The southern UKST plates have a limiting magnitude of 22.5 in B and 21 in R. The APM objects near FIRST objects were identified for the entire 2001 October 15 FIRST catalog (see McMahon et al. 2002). We searched for all APM objects within $5''$ of the radio lobes on our list, and also noted any counterparts to the radio cores. In addition, we searched the SDSS Early Data Release (Stoughton et al. 2002), which covered only 462 square degrees but was complete to 22.2 in r , in a similar manner. These searches identified 4500 lobes with coincident optical objects. Since this number was too large for a realistic follow-up campaign, we further narrowed the list to 380 candidates by requiring the radio lobes be brighter than 100 mJy at 20 cm, which allowed for the most efficient follow-up radio observations.

To make the final cut, three of us (D.B.H., J.L., J.N.W.) visually inspected the targets selected by the computer algorithm. We checked that the FIRST radio morphology was consistent with a double-lobed radio galaxy, and that the optical object appeared to be real (rather than an image artifact) and was indeed well aligned with a lobe. Objects were deemed better targets if the optical counterpart was red or extended (making it more likely to be a galaxy, rather than a foreground star), and if a separate optical object was coincident with the radio core (since this would facilitate redshift determination of the radio galaxy). With these criteria we selected 92 targets for high-resolution follow-up VLA observations.

3. Radio Observations

We obtained high-resolution VLA images for all 92 targets. The goals of this step of the survey were to confirm that the FIRST source really is a radio lobe, to obtain a more accurate radio position for comparison with the catalog position of the optical object, and to look for lensed structures (e.g., rings, arcs, and multiple images) on the expected scale of $\sim 1''$. Table 1 gives the coordinates, exposure time, and observing wavelength for each of the VLA observations. Of these, 11 had been previously observed and were available in the VLA archive or the literature. The remaining 81 targets were observed over 32.5 hours in four sessions in March 2002. These observations took place when the VLA was in the A configuration, and employed the standard 6 cm (5 GHz) band, giving a synthesized beam size of $\sim 0''.4$ FWHM. A bandwidth of 100 MHz was recorded for each circular polarization. The data were calibrated with standard AIPS⁸ procedures. The flux density scale was set using 3C 286 and 2355+498, and the polarization was calibrated using 1310+323 and 2355+498. The data were mapped and deconvolved using the standard CLEAN algorithm, and two rounds of self-calibration were applied to the antenna phases.

In the resulting maps, 9 targets were unresolved, suggesting that they are actually radio cores rather than lobes. Another 53 targets were indeed lobes, but the more accurate radio position showed that the lobe emission did not coincide with the catalog position of the optical object. The remaining 30 candidates were re-mapped using the multi-scale CLEAN (MSC) deconvolution algorithm (Wakker & Schwarz 1988) and are shown in Figure 1. The standard CLEAN algorithm tends to introduce point-like artifacts (a “pebbly” look) into extended radio sources, because it models the sky as a set of point sources, which is a poor approximation for diffuse radio lobes. The MSC algorithm assumes the sky is composed of both points and elliptical Gaussian components of various dimensions. Using MSC, we were able to reduce the artifacts in the maps and provide a more realistic description of the actual radio source. The rms noise in the MSC-deconvolved maps ranged from 35 to 90 $\mu\text{Jy beam}^{-1}$, and was usually less than 60 $\mu\text{Jy beam}^{-1}$.

In at least 24 of these 30 cases, there was a radio point source positioned between the lobes, presumably the core of the radio galaxy. An optical counterpart to this radio point source was present in 18 cases, which was used for more precise registration of the radio and optical images.

4. Optical Observations

In the next phase of the survey, we obtained CCD optical images of all 30 candidates, in order to confirm the existence of the optical counterpart and eliminate spurious catalog entries, to obtain a more accurate optical position and test whether it truly coincides with the radio lobe, and to confirm that it is a galaxy rather than a star by measuring its angular extent. Table 2

⁸The Astronomical Image Processing System (AIPS) is developed and distributed by the National Radio Astronomy Observatory.

summarizes the follow-up optical observations, which took place from 2002 through 2004, using a variety of telescopes and cameras. In some cases we obtained images of a single candidate using more than one telescope, but in what follows we describe only the images with the best seeing and signal-to-noise ratio.

Fourteen candidates were imaged with the 4-shooter CCD camera on the FLWO 1.2 meter telescope⁹, for 1200 seconds in each of V and I bands. Two candidates were imaged with the MagIC camera on the 6.5 m Baade Magellan Telescope¹⁰ in the g' and i' bands. Seven candidates were imaged at the MDM 2.4 meter Hiltner Telescope¹¹ in the I band for 900 to 1800 seconds each. Finally, for 7 candidates, the best available CCD images were drawn from the SDSS Data Release 1 (DR1) and Data Release 2 (DR2), which were made public after our VLA observations. Among the SDSS data products is a classification of each object as either pointlike or extended, which is deemed reliable for objects with r magnitude brighter than 21. We provide these results, where available, in Table 2 and Figure 1.

In those cases for which the core was detected at both optical and radio wavelengths, the images were registered by requiring coincidence of the optical and radio core. If this was not possible, then the VLA radio position was matched to the SDSS optical position (or a plate solution using USNO-B1.0 stars¹², for cases in which the SDSS position was not available).

Because two of the 30 candidate radio galaxies have an optical counterpart to both lobes, there are a total of 32 candidate lens galaxies in our sample. Nine of the 32 candidates were eliminated through optical follow-up: one is a spurious catalog entry, three are not coincident with the radio lobe, and five are stellar. Most of the remaining lens candidates have non-stellar optical counterparts that are well aligned with a radio lobe (see Table 3).

In a few cases, redshifts of either the radio galaxy or the candidate lens galaxy were already known. We searched the NASA/IPAC Extragalactic Database¹³, finding redshifts for 5 core counterparts and 3 candidate lens galaxies. These redshifts are given in Table 3 and Figure 1. We also searched SDSS DR1 and DR2 for redshifts of our candidate objects, but we did not find any additional information.

⁹The Fred Lawrence Whipple Observatory (FLWO) is a facility of the Smithsonian Institution.

¹⁰The 6.5 m Baade telescope is one of the two telescopes of the Magellan Project, a collaboration between Carnegie Observatories, the University of Arizona, Harvard University, the University of Michigan, and the Massachusetts Institute of Technology.

¹¹The MDM Observatory is owned and operated by University of Michigan, Dartmouth College, Ohio State University, and Columbia University.

¹²The USNOFS Image and Catalogue Archive is operated by the United States Naval Observatory, Flagstaff Station, <http://www.nofs.navy.mil/data/fchpix/>.

¹³The NASA/IPAC Extragalactic Database (NED) is operated by the Jet Propulsion Laboratory, California Institute of Technology, under contract with the National Aeronautics and Space Administration.

5. Target FOV J0743+1553

The results for all 32 candidate lens galaxies are discussed in the next section. One of the targets, FOV J0743+1553, captured our interest because at 6 cm the morphology is suggestive of a doubly-imaged hot spot (Figure 1a). Furthermore, the optical counterpart proved to be a spiral galaxy, raising the prospect of the discovery of a rare case in which a spiral galaxy acts as a gravitational lens. Our follow-up observations are described below, along with a description of the strengths and weaknesses of the lensing hypothesis.

5.1. A spiral galaxy

Ground-based images revealed the optical counterpart to FOV J0743+1553 to be highly elliptical and suggestive of a disk galaxy. We obtained images with higher angular resolution using the *Hubble Space Telescope* (*HST*), under the auspices of the CASTLES¹⁴ project. Optical images (using filters F814W and F555W) were obtained on 2003 September 10 with the Advanced Camera for Surveys (ACS). Near-infrared images were obtained on 2003 October 6 with the Near Infrared Camera and Multi-Object Spectrometer (NICMOS) using the F160W filter. The 4 dithered exposures obtained through each filter were combined, using the MultiDrizzle software (Koekemoer et al. 2002) for the ACS exposures and the NICRED software (Lehár et al. 2000) for NICMOS exposures. The final images are displayed in Figures 4 and 5.

These images confirmed that the optical counterpart is a spiral galaxy. The galaxy is highly elongated and has pronounced dust lanes that are most obvious in the bluest (F555W) image. The galaxy is viewed somewhat edge-on; given its aspect ratio, the inclination is approximately 60 degrees. We found that the H band (F160W) surface brightness distribution is well described by a combination of two analytic functions: a de Vaucouleurs profile, representing the bulge, and an exponential profile, representing the disk. The parameters of the best-fitting model of the surface brightness are given in Table 4.

We also obtained an optical spectrum of the galaxy using the 6.5m telescope at the MMT Observatory¹⁵ in 2002 April. The spectrum, reduced in the standard manner with IRAF, is shown in Figure 3. There are emission lines of o III, H α and o II, as well as absorption features due to hydrogen and alkali metals, all at a redshift of 0.1918 ± 0.0002 . The nebular lines are consistent with a spiral galaxy.

The rarity of spiral lenses makes the prospect of discovering a new spiral lens especially appealing. The sample of known lensing galaxies is overwhelmingly dominated by massive elliptical galaxies. Spiral galaxies have a smaller lensing cross-section than elliptical galaxies and are less

¹⁴The CfA–Arizona Space Telescope Lens Survey (CASTLES) Kochanek et al. 2000a

¹⁵The MMT Observatory is a joint facility of the Smithsonian Institution and the University of Arizona.

likely to be found as lenses. Of the roughly 90 lens systems listed by CASTLES, only five are known to be spiral galaxies (see Winn, Hall, & Schechter 2003 for a summary of spiral lenses). For several of the known spiral galaxy lens systems, accurate photometry of the lens galaxy is difficult because the field is very crowded or the quasar images are very bright, but FOV J0743+1553 does not suffer from those problems. Unfortunately, the hypothesis that spiral galaxy FOV J0743+1553 is a case of lensing is problematic. In what follows, we summarize the evidence for and against this hypothesis.

5.2. The case for lensing

The morphology of the radio source at 6 cm is compatible with the lensing interpretation. The southern lobe, shown in Figure 2), consists of a faint ring and several brighter components. Two components of the ring, labeled A and B, are $1''.8$ apart in a roughly north–south direction. These can be interpreted as two lensed images of the same region of radio emission in the background lobe. These components bracket the position of the foreground galaxy. The fainter component is closer to the galaxy centroid, as expected from lensing theory. Furthermore, components A and B have similar fractional polarizations, and similar polarization angles. These properties are natural consequences of gravitational lensing, but are not necessarily expected of two distinct hot spots in a radio lobe. The other parts of the southern lobe—the bright region on the southwest side of the lobe, and the jet extending to the core to the northeast—have different polarizations, and are thus unlikely to represent multiple images of a single source.

It is possible to make a simple model for the mass distribution of the lens galaxy and the intrinsic radio source structure that is compatible with the 6 cm data. The dark matter halo of the spiral galaxy is modeled as a singular isothermal sphere with an Einstein radius of $\sim 1''.8$. The model is shown in Figure 7. The upper right panel shows the model of the intrinsic 6 cm radio source structure (a sum of 7 elliptical Gaussian functions), while the upper left panel shows the lensed source. The center of the mass distribution was adjusted (within the error uncertainty of the radio–optical registration) until the model provided a good visual fit to the observed radio morphology; the mass is centered $0''.03$ east and $0''.45$ south of component B. This model is offered as an “existence proof,” rather than a unique solution. It demonstrates that a foreground mass would be able to lens a portion of the lobe into images A and B without producing multiple images in other parts of the lobe. The hypothesized source structure is reasonable; it is reminiscent of many radio jets and lobes.

5.3. The case against lensing

Radio lobes show a great diversity in morphology. For this reason, a lens-like morphology is not sufficient as proof that gravitational lensing is occurring. In contrast, the situation with flat-

spectrum sources is often clearer, especially in the case of quadruply-imaged quasars, since there are no other known types of radio source that exhibit 4 compact flat-spectrum components. In radio lobes, hot spots and filaments can be arranged to look like multiple images or rings, even when no lens galaxy is detected in optical or infrared. Two examples in the literature are 4C 39.24 (Law-Green et al. 1995) and MG 0248+0641 (Conner et al. 1998); some additional examples are given in § 6 (FOV J1508+0102 and FOV J1613+3724). The bottom line is that additional evidence beyond morphology is particularly important.

The lensing hypothesis requires that the radio source be behind the spiral galaxy. Unfortunately, the redshift of this radio galaxy cannot be measured, because the optical counterpart to the compact radio core has not been detected (the radio core is northeast of the lobe, Figure 1a). Our most constraining upper limit on the brightness of an optical point source is $I > 26$, from the *HST* ACS image. Statistically, FIRST radio lobes tend to have redshift $z \sim 1$ (Cress & Kamionkowski 1998), which is greater than the redshift of the spiral galaxy ($z = 0.19$). But without a redshift measurement of this particular radio source, we cannot confirm whether it is in the background or the foreground of the spiral galaxy. This certainly reduces the confidence one can place in any particular interpretation of the system. The lack of a detectable optical counterpart also inhibits the accuracy of the optical–radio registration; we have registered the optical and radio images using astrometry from the VLA observation and stars from the USNO-B1.0 catalog.

Lensing preserves the spectrum of a background object. For this reason, the multiple images of a gravitational lens will have the same arrangement and relative flux densities regardless of the observing frequency¹⁶, whereas the intrinsic source structure of radio lobes can vary dramatically with frequency. We observed FOV J0743+1553 at 18 cm in order to test whether the lens-like morphology persists at longer wavelengths. We used MERLIN¹⁷ for 50 hours in 4 sessions in 2003 February and April. We employed the standard 1.65 GHz band, with a bandwidth of 15 MHz per polarization. The data were calibrated using standard procedures in AIPS, and the mapping was performed with CLEAN deconvolution and two iterations of self-calibration (Figure 6). The 18 cm image shows a string of compact components across the south side of the lobe, and faint over-resolved emission in the rest of the lobe. The positions of the southern compact components agree well with the position of the brightest emission on the south side of the VLA 6 cm image. The north side of the lobe, however, does not show significant compact emission at the VLA position of the B image. Thus, the flux ratio of the A and B images is significantly different at the two wavelengths (A/B is 1.9 at 6 cm, but at least 3.0 at 18 cm), in contrast to lensing theory and to our simple model (the 18 cm model is shown in the lower panels of Figure 7). This does not strictly

¹⁶We note that in some relatively rare cases, differential propagation effects such as scatter-broadening and free-free absorption can complicate this test of the lensing hypothesis (see, e.g., Sykes et al. (1998); Biggs et al. (2004); Winn et al. (2004)).

¹⁷The Multi-Element Radio Linked Interferometer Network (MERLIN) is a UK national facility operated by the University of Manchester at Jodrell Bank Observatory on behalf of PPARC.

rule out the lensing hypothesis, since it could be viable with some elaboration, such as preferential free-free absorption of image B. However, in the absence of independent evidence for such an effect, the lensing hypothesis is certainly less satisfying.

Another useful test is whether the mass of the galaxy as implied by lensing theory is at least approximately equal to the mass of the galaxy as inferred from its luminosity. The Tully-Fisher relation is an empirical correlation between absolute magnitude and circular velocity, and circular velocity can be taken as a proxy for mass. The following calculation is similar to that described more fully in Winn et al. (2002a). An isothermal sphere producing the $1''.8$ image separation between A and B would cause a flat rotation curve with circular velocity 286 km s^{-1} (assuming the radio galaxy is at redshift 1). Using the Tully-Fisher relation of Sakai et al. (2000), this corresponds to an aperture absolute magnitude of the galaxy’s disk of -24.6 ± 0.4 in rest-frame H-band. We observed the H-band apparent magnitude of the total disk to be 16.20 ± 0.04 (Table 4). After an aperture correction of $2.5 \log_{10} 2$ (Aaronson et al. 1982; Sakai et al. 2000), a K-correction of 0.065 mag (as appropriate for an early type spiral with star formation starting at redshift ~ 1.5), and a 0.017 mag correction for Galactic extinction (Schlegel et al. 1998), the absolute magnitude is estimated to be -22.79 ± 0.04 . This is 1.8 ± 0.4 magnitudes (nearly 5σ) fainter than expected for a galaxy that is sufficiently massive to be acting as a gravitational lens. (This result is relatively independent of source redshift: for $z = 2$ the discrepancy is still greater than 4σ , and for $z = 0.3$ the difference is over 7σ .) Either the galaxy follows the Tully-Fisher relation and does not have enough mass to produce images A and B, or it has a much higher mass-to-light ratio than the local galaxies on which the Tully-Fisher relation is based.

On balance, the case against lensing seems stronger than the case for lensing. The 6 cm morphology is certainly suggestive but the 18 cm morphology does not obey the simplest lensing prediction, and the mass of the galaxy as predicted by the Tully-Fisher relation is insufficient to produce the $1''.8$ image splitting. Additional observations could confirm or deny the multiple-image interpretation with more certainty. For instance, detection of an optical core and its photometric redshift could determine whether the radio lobe is more distant than the spiral galaxy, and provide precise alignment for better modeling. Higher resolution images at 6 cm would be sensitive to fine structure in the lobe and could test whether the regions A and B are as similar as they appear at lower resolution.

6. Other Targets

In this section we discuss other targets in the survey. The status of each of the 32 lens galaxy candidates is given in Table 3. Here we describe some candidates in more detail. These have features that initially suggested lensing or atypical lobes, prompting additional consideration or followup observations. None, however, turned out to be a promising lens candidate worth further study.

FOV J0822+4412: (Figure 1b) There are two radio components in the field, but it is unclear if they are physically related to one another. The middle of the eastern component is associated with an unresolved SDSS optical object that may be the active nucleus of the radio galaxy. The western radio source is extended, with an optical object having similar extent at the same position; this radio emission is smooth with no sign of lensing or a ring. The western object could be a lobe of the eastern AGN with an optical galaxy along the line of sight, or the western radio and optical emission may originate from the same object, such as a starburst galaxy.

FOV J0952+0000: (Figure 1b) The core of this radio galaxy has an optical counterpart, giving a source redshift of 1.06 and precise optical-radio registration. The western jet has a $2''.5$ gap at the position of an extended optical object at unknown redshift. If this galaxy is in the foreground, the gap in the jet may be due in part to lensing (emission on either side of the gap could be images of the same background source), or it could be an unlensed jet with coincidental placement of the galaxy. The radio feature is quite faint, and much deeper radio imaging would be required to begin to separate the intrinsic shape of the jet from lensing effects.

FOV J1108+0202: (Figure 1c) The eastern radio source has two closely spaced components on either side of an extended optical object. A polarization image (Figure 9), however, shows that the two radio components have significantly different fractional polarization and are very unlikely to be lensed images of a single source.

FOV J1108–0038 N: (Figure 1d) The northern lobe of this radio galaxy has an arc structure (about 3 arcseconds in diameter), but the polarization map shows significantly different polarization along the arc (Figure 10). This polarization is typical of radio lobes, with the electric field perpendicular to the shock front. Thus the arc is much more simply explained as an intrinsic radio structure rather than a lensed lobe with Faraday rotation along the arc.

FOV J1253+0238: (Figure 1d) The optical object is extended (a galaxy), and coincident with a knot of radio emission. This knot could be a hot spot in the jet, possibly lensed by a galaxy in the foreground. The optical-radio alignment suggests, however, that the radio knot is the asymmetric core of the radio galaxy, emitting jets to the northwest and southeast. The optical emission is mostly likely from the AGN host galaxy at the same redshift.

FOV J1316+0025: (Figure 1d) A faint optical object ($r = 22.2$) is coincident with a bright smooth part of the western radio lobe in the VLA image (Figure 1). The core was detected at both optical and radio wavelengths, allowing for precise registration. We observed this lobe at 18 cm using MERLIN on four dates in 2003 April and May. The data were calibrated using standard techniques, and mapped using a maximum entropy deconvolution algorithm (VTESS) and self-calibration (Figure 11). This high resolution map shows that the optical counterpart is located far from the brightest part of the lobe, and that there are no obvious lensed structures around it.

FOV J1508+0102: The eastern lobe has a ring-like appearance in the VLA 6 cm map (Figure 8). Initial optical followup showed the optical counterpart to be extended and slightly offset from the center of the radio ring. The radio morphology was confirmed in an 18 cm MERLIN

observation in 2003 March, lasting 12 hours. Comparison of the 6 cm and 18 cm maps shows that the spectral index is similar for all the bright components of the ring, consistent with a lensing interpretation. Later optical images (with improved seeing) showed, however, that the optical counterpart is two unresolved objects, presumably a binary star. It is possible that the lobe is lensed but the lens galaxy is too faint to have been detected in current CCD images, but it is also possible that it is an unlensed lobe with unusual morphology. Additional study is not warranted, because even if it were lensed, the faintness of the lens galaxy would make observations very difficult.

FOV J1613+3724: This object was originally selected because the optical and radio catalog positions were coincident at the northwest lobe. Radio followup showed that the lobe was clearly south of the optical catalog position (Figure 1g). The ring-like shape of the lobe prompted us to pursue optical followup anyway. Unfortunately, no optical emission was detected within the radio ring shape, and (similar to FOV J1508+0102) further study is not warranted.

7. Summary

The basic premise of our lensed lobe survey is that gravitational lens candidates can be selected with relatively high efficiency from existing wide-field radio and optical catalogs, by requiring radio sources that appear to be lobes of radio galaxies to be nearly coincident with optical sources that appear to be galaxies. We have developed a selection algorithm for this purpose that is tailored to the FIRST radio catalog, and either the APM or SDSS optical catalogs. The superior depth and angular resolution of the SDSS catalog, in particular, makes some of the optical follow-up observations redundant, by greatly reducing the rate of false positive optical detections and allowing a much stronger discrimination between stars and galaxies.

In the previous round of this survey, using FIRST and APM, Lehár et al. (2001) identified one new lens and recovered one previously known lens out of a sample of 33 candidate lensed lobes. In this round, we selected an additional 92 candidate lensed lobes, mainly from FIRST and APM but also using a subset of the SDSS catalog. After follow-up observations with higher angular resolution at both radio and optical wavelengths, we found 16 galaxies nearly coincident with radio lobes, but these do not appear to be lensed. We found two ring-shaped radio lobes, but detected no coincident optical galaxy (FOV J1508+0102 and J1613+3724). We found only one possible gravitational lens (FOV J0743+1553), but even in this case, the lensing interpretation is problematic. We must admit that this round of the survey was not as successful in finding lenses as we had expected, based on the first round. This warrants a reconsideration of the basic premise underlying the survey.

Some of the challenges we experienced are based on an inherent difficulty of any systematic study of radio lobes: their morphologies are sometimes peculiar. This makes it difficult to establish with a high level of confidence that a promising candidate is actually gravitationally lensed, rather than simply exhibiting an intrinsically lens-like morphology (an arc, a ring, or multiple blobs). An additional challenge that is common to all radio lens surveys is that the source redshift can be

extremely difficult to measure. The radio core must be detected and its optical counterpart must be bright enough for spectroscopy. This is not usually a problem in optical lens surveys, for which the sources are (by design) bright quasars with prominent emission lines.

Nevertheless, lensed lobes are worth pursuing because they are plentiful and useful. They are plentiful because of the large angular sizes of lobes relative to cores; they should constitute $\sim 75\%$ of all radio lenses (Kochanek & Lawrence 1990). They are useful, at least in principle, because observations of lensed extended sources provide more information about the foreground mass distribution than lensed point sources. To reap the benefits of lensed lobes, a survey strategy needs to compensate for the difficulties discussed above by efficiently producing large numbers of promising candidates, and in particular, candidates that can be examined at high angular resolution with a high signal-to-noise ratio.

Our pre-selection process did successfully find optical galaxies that are nearly coincident with radio lobes (at least 17 out of 92 candidates). But, counter to our expectations, none of these 17 objects could be confidently interpreted as a case of gravitational lensing. Why is this the case? In retrospect, we can offer some plausible speculations. (1) The assumption that the galaxy is in the foreground of the radio source may be incorrect. This assumption seems reasonably well justified because the typical FIRST radio source has a redshift of order unity, while the typical APM or SDSS galaxy has redshift of ~ 0.1 . But there will surely be counter-examples. For radio sources that are in clusters of galaxies, the optically detected galaxy may be at nearly the same redshift as the radio source. This may happen more often than one would naively expect, since a massive galaxy is somewhat more likely to be a radio galaxy if it is in a cluster, than if it is isolated. (2) The Einstein radius of the optically detected galaxy may be too small to produce multiple images or strong shearing of the background source, whether because of a small galactic mass or an unfavorable combination of distances between the lens and source. For the typical masses and redshifts in the parent catalogs of our sample, Einstein rings would be easily detectable at the resolution of our VLA observations. For at least some of the actual targets we observed, the relative lens and source distances would produce an Einstein ring too small for us to detect. (3) The surface brightness distribution of the radio lobe may not have enough contrast on arcsecond scales. If the surface brightness distribution is too smooth on the angular size of the Einstein ring, then gravitational lensing does not produce a detectable effect.

There is another respect in which our pre-selection process was efficient: we were generally successful in identifying radio lobes based on the limited morphological information of the comparatively low-resolution FIRST catalog. Our VLA observations of the 92 targets showed that 83 of them were indeed lobes of radio galaxies. Unfortunately none of these could be shown definitively to be gravitationally lensed. As mentioned above, the lobe must vary in brightness over angular sizes comparable to the Einstein radius, or the Einstein ring will not appear. Yet the resolution of FIRST is several times larger than the typical Einstein radius for our sample, and hence FIRST cannot be used to pre-select lobes with sufficient contrast. Conversely, some lobes that are nearly unresolved in FIRST (and that might consequently be missed by our selection al-

gorithm) might have sufficient contrast on arcsecond scales. Several previously discovered lensed lobes (MG 0751+2716, MG 1131+0456, and MG 1654+1346) appear unresolved or only slightly extended in FIRST images.

Finally, even after drawing up a shortlist of candidates of definite radio lobes with a definite candidate lens galaxy in the foreground, the task still remains to obtain radio images with both high angular resolution and high sensitivity. This must be done not only to confirm that an object is lensed, but also to reap the benefits of the lensed extended structures as modeling constraints, which is the primary scientific motivation. Here the difficulty is that high angular resolution generally means high-frequency observations (for a given interferometer), and because the intrinsic radio spectra of radio lobes generally decline sharply with frequency, the requirement of high angular resolution is at odds with the requirement for high sensitivity. We believe that a successful survey for lensed lobes will require a new generation of radio interferometers, capable of rapid, high-resolution imaging of steep-spectrum objects. With current instruments, we have demonstrated that a careful pre-selection of candidates reduces the total telescope time needed for the initial phase of a lens survey, but the radio follow-up observations that are needed to realize the benefits of lensed lobes are (at least in the cases we have discovered in this round of the survey) prohibitively expensive. Work is underway on the future instruments that would be appropriate, such as the expanded VLA and e-MERLIN, and in the more distant future, the Square Kilometer Array¹⁸ would be an outstanding tool to find and characterize gravitationally lensed radio lobes.

We are grateful to our referee for constructive criticism. We thank Ari Buchalter for assistance with FIRST catalog search software, Richard McMahon for assistance with the APM-FIRST catalog, Ashish Mahabel for assistance with the DPOSS catalog, David Rusin for observations at Magellan, and Don Terndrup for observations at MDM. D.B.H. was supported by a Cottrell College Science Award from Research Corporation. For part of this work, J.N.W. was supported by an NSF Astronomy and Astrophysics Postdoctoral Fellowship under award AST-0104347, and subsequently by NASA through Hubble Fellowship grant HST-HF-01180.02-A, awarded by the Space Telescope Science Institute, which is operated by the Association of Universities for Research in Astronomy, Inc., for NASA, under contract NAS 5-26555. C.S.K. is supported by NASA ATP grant NAG5-9265. This work is based on observations made with the NASA/ESA Hubble Space Telescope, obtained at the Space Telescope Science Institute, which is operated by AURA, Inc. under NASA contract NAS5-26555; the observations are part of HST program GO-9744.

REFERENCES

Aaronson, M., Huchra, J., Mould, J. R., Tully, R. B., Fisher, J. R., et al. 1982, ApJ, 50, 241

¹⁸www.skatelescope.org

- Becker, R. H., White, R. L., & Helfand, D. J. 1995, *ApJ*, 450, 559
- Biggs, A. D., Browne, I. W. A., Jackson, N. J., York, T., Norbury, M. A., McKean, J. P., & Phillips, P. M. 2004, *MNRAS*, 350, 949
- Browne, I. W. A. et al. 2003, *MNRAS*, 341, 13
- Burke, B. F., Conner, S. R., Hewitt, J. N., & Lehar, J. 1993, in *Sub-arcsecond Radio Astronomy*, ed. R. J. Davis & R. S. Booth (Cambridge: Cambridge University Press), 123
- Chae, K. & Mao, S. 2003, *ApJ*, 599, L61
- Cohn, J. D., Kochanek, C. S., McLeod, B. A., & Keeton, C. R. 2001, *ApJ*, 554, 1216
- Conner, S. R., Cooray, A. R., Fletcher, A. B., Burke, B. F., Lehar, J., Garnavich, P. M., Muxlow, T. W. B., Thomasson, P., & Blakeslee, J. P. 1998, *AJ*, 115, 37
- Courbin, F., Saha, P., & Schechter, P. L. 2002, in *Lecture Notes in Physics*, Vol. 608, *Gravitational Lensing: An Astrophysical Tool*, ed. F. Coubin & D. Minniti, 1
- Cress, C. M. & Kamionkowski, M. 1998, *MNRAS*, 297, 486
- Davis, A. N., Huterer, D., & Krauss, L. M. 2003, *MNRAS*, 344, 1029
- Fukugita, M., Futamase, T., Kasai, M., & Turner, E. L. 1992, *ApJ*, 393, 3
- Gregg, M. D., Becker, R. H., Schechter, P. L., White, R. L., & Wisotzki, L. 2000, *BAAS*, 32, 1578
- Hewitt, J. N., Turner, E. L., Schneider, D. P., Burke, B. F., & Langston, G. 1988, *Nature*, 333, 537
- Jauncey, D. L., Reynolds, J. E., Tzioumis, A. K., Murphy, D. W., Preston, R. A., Jones, D. L., et al. 1991, *Nature*, 352, 132
- Keeton, C. R., Kochanek, C. S., & Seljak, U. 1997, *ApJ*, 482, 604
- Kochanek, C. S. 1991, *ApJ*, 373, 354
- . 2003, *ApJ*, 583, 49
- Kochanek, C. S., Falco, E. E., C. Impey, Lehar, J., McLeod, B., & Rix, H.-W. 2000a, the CASTLES survey, <http://cfa-www.harvard.edu/glensdata>
- Kochanek, C. S., Falco, E. E., Impey, C. D., Lehar, J., McLeod, B. A., Rix, H.-W., Keeton, C. R., Muñoz, J. A., & Peng, C. Y. 2000b, *ApJ*, 543, 131
- Kochanek, C. S. & Lawrence, C. R. 1990, *AJ*, 99, 1700
- Kochanek, C. S., Schneider, P., & Wambsganss, J. 2004, in *Gravitational lensing: Strong, Weak, and Micro*, Proceedings of the 33rd Saas-Fee Advanced Course, ed. P. J. . P. N. G. Meylan (Berlin: Springer-Verlag)

- Koekemoer, A. M., Fruchter, A. S., Hook, R., & Hack, W. 2002, in HST Calibration Workshop, ed. S. Arribas, A. Koekemoer, & B. Whitmore (Baltimore: Space Telescope Science Institute), 381
- Langston, G. I., Schneider, D. P., Conner, S. R., Carilli, C. L., Lehár, J., Burke, B. F., Turner, E. L., Gunn, J. E., Hewitt, J. N., & Schmidt, M. 1989, *AJ*, 97, 1283
- Law-Green, J. D. B., Eales, S. A., Leahy, J. P., Rawlings, S., & Lacy, M. 1995, *MNRAS*, 277, 995
- Lehár, J., Buchalter, A., McMahon, R. G., Kochanek, C. S., & Muxlow, T. W. B. 2001, *ApJ*, 547, 60
- Lehár, J., Burke, B. F., Conner, S. R., Falco, E. E., Fletcher, A. B., Irwin, M., McMahon, R. G., Muxlow, T. W. B., & Schechter, P. L. 1997, *AJ*, 114, 48
- Lehár, J., Falco, E. E., Kochanek, C. S., McLeod, B. A., Muñoz, J., Impey, C. D., Rix, H.-W., Keeton, C. R., & Peng, C. Y. 2000, *ApJ*, 536, 584
- Lehár, J., Langston, G. I., Silber, A., Lawrence, C. R., & Burke, B. F. 1993, *AJ*, 105, 847
- Maoz, D., Bahcall, J. N., Schneider, D. P., Bahcall, N. A., Djorgovski, S., Doxsey, R., Gould, A., Kirhakos, S., Maylan, B., & Yanny, B. 1993, *ApJ*, 409, 28
- McMahon, R. G., White, R. L., Helfand, D. J., & Becker, R. H. 2002, *ApJS*, 143, 1
- Morgan, N. D., Caldwell, J. A. R., Schechter, P. L., Dressler, A., Egami, E., & Rix, H.-W. 2004, *AJ*, 127, 2617
- Narayan, R. & Bartelmann, M. 1999, in *Formation of Structure in the Universe*, ed. A. Dekel & J. P. Ostriker (Cambridge: Cambridge University Press), 360
- Ofek, E. O., Rix, H., & Maoz, D. 2003, *MNRAS*, 343, 639
- Oguri, M. et al. 2005, *ApJ*, 622, 106
- Patnaik, A. R., Browne, I. W. A., King, L. J., Muxlow, T. W. B., Walsh, D., & Wilkinson, P. N. 1993, *MNRAS*, 261, 435
- Rusin, D., Kochanek, C. S., Falco, E. E., Keeton, C. R., McLeod, B. A., Impey, C. D., Lehár, J., Muñoz, J. A., Peng, C. Y., & Rix, H.-W. 2003a, *ApJ*, 587, 143
- Rusin, D., Kochanek, C. S., & Keeton, C. R. 2003b, *ApJ*, 595, 29
- Rusin, D. & Ma, C. 2001, *ApJ*, 549, L33
- Rusin, D., Norbury, M., Biggs, A. D., Marlow, D. R., Jackson, N. J., Browne, I. W. A., N. Wilkinson, P., & Myers, S. T. 2002, *MNRAS*, 330, 205

- Sakai, S., Mould, J. R., Hughes, S. M. G., Huchra, J. P., et al. 2000, *ApJ*, 529, 698
- Schlegel, D. et al. 1998, *ApJ*, 500, 525
- Stoughton, C. et al. 2002, *AJ*, 123, 485
- Sykes, C. M., Browne, I. W. A., Jackson, N. J., Marlos, D. R., Nair, S., Wilkinson, P. N., et al. 1998, *MNRAS*, 301, 310
- Trotter, C. S., Winn, J. N., & Hewitt, J. N. 2000, *ApJ*, 535, 671
- Turner, E. L. 1990, *ApJ*, 365, L43
- van de Ven, G., van Dokkum, P. G., & Franx, M. 2003, *MNRAS*, 344, 924
- Wakker, B. P. & Schwarz, U. J. 1988, *A&A*, 200, 312
- Winn, J. N. 2001, *phD Thesis*, MIT
- Winn, J. N., Hall, P. B., & Schechter, P. L. 2003, *ApJ*, 597, 672
- Winn, J. N., Kochanek, C. S., McLeod, B. A., Falco, E. E., Impey, C. D., & Rix, H.-W. 2002a, *ApJ*, 575, 103
- Winn, J. N., Morgan, N. D., Hewitt, J. N., Kochanek, C. S., Lovell, J. E. J., Patnaik, A. R., Pindor, B., Schechter, P. L., & Schommer, R. A. 2002b, *AJ*, 123, 10
- Winn, J. N., Rusin, D., & Kochanek, C. S. 2004, *Nature*, 427, 613
- Wisotzki, L., Schechter, P. L., Chen, H.-W., Richstone, D., Jahnke, K., Sánchez, S. F., & Reimers, D. 2004, *A&A*, 419, L31

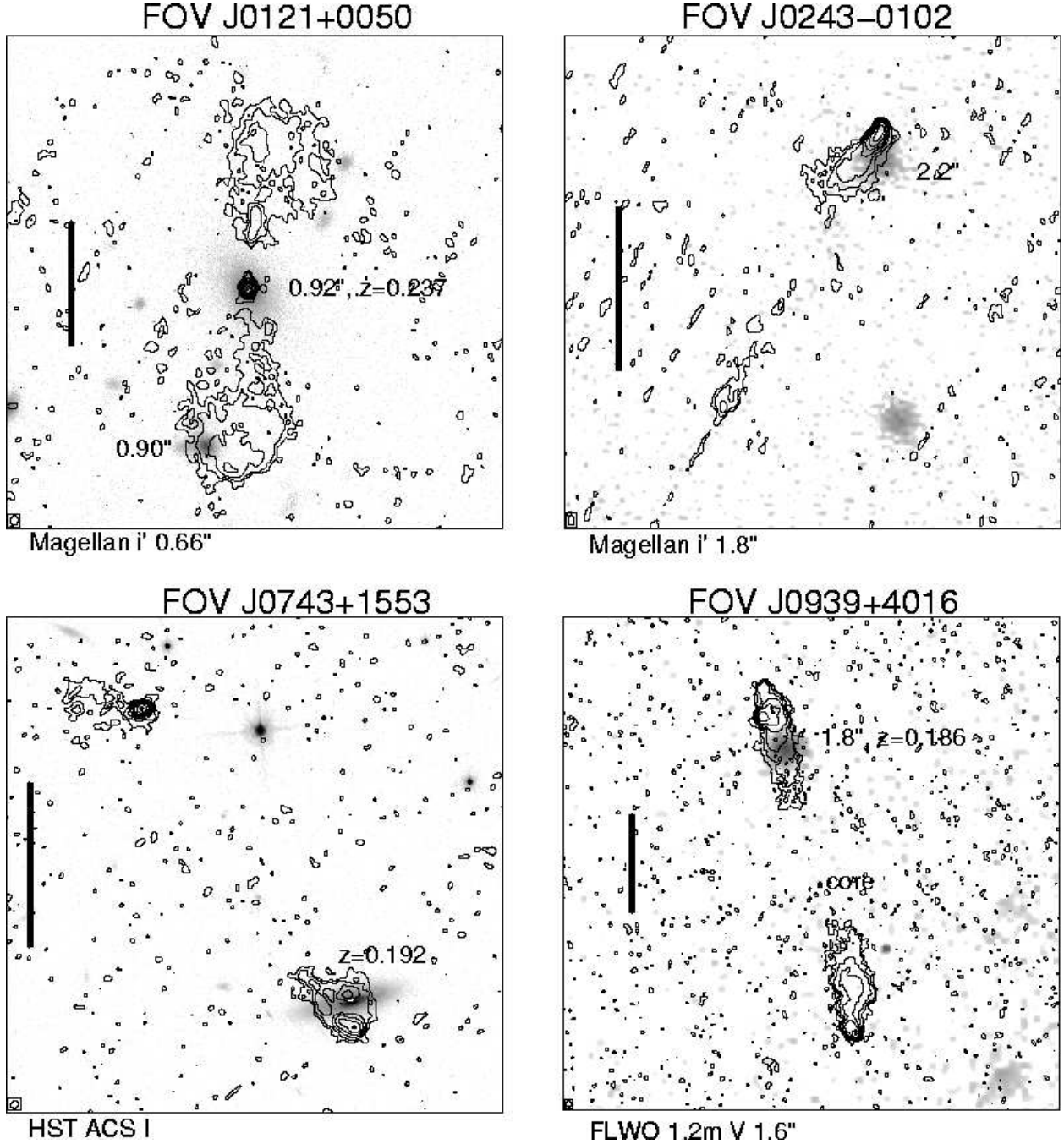


Fig. 1a.— Radio and optical maps of the top 30 candidates. North is up and east is to the left. The vertical bars are 10 arcseconds long. The contours are VLA data, with contour levels increasing by doubling from twice the off-source map rms; the beam is shown in the lower left. The optical data is shown in a square-root grey scale selected to highlight the potential lens and/or core counterpart, and the telescope, filter, and seeing is given in the lower left. The measured FWHM extent of certain optical objects is indicated in the images. For SDSS data, designations of “point” and “extended” are shown for brighter objects ($r < 21$). Crosses indicate the position of optical catalog objects which are not clearly visible in the optical image.

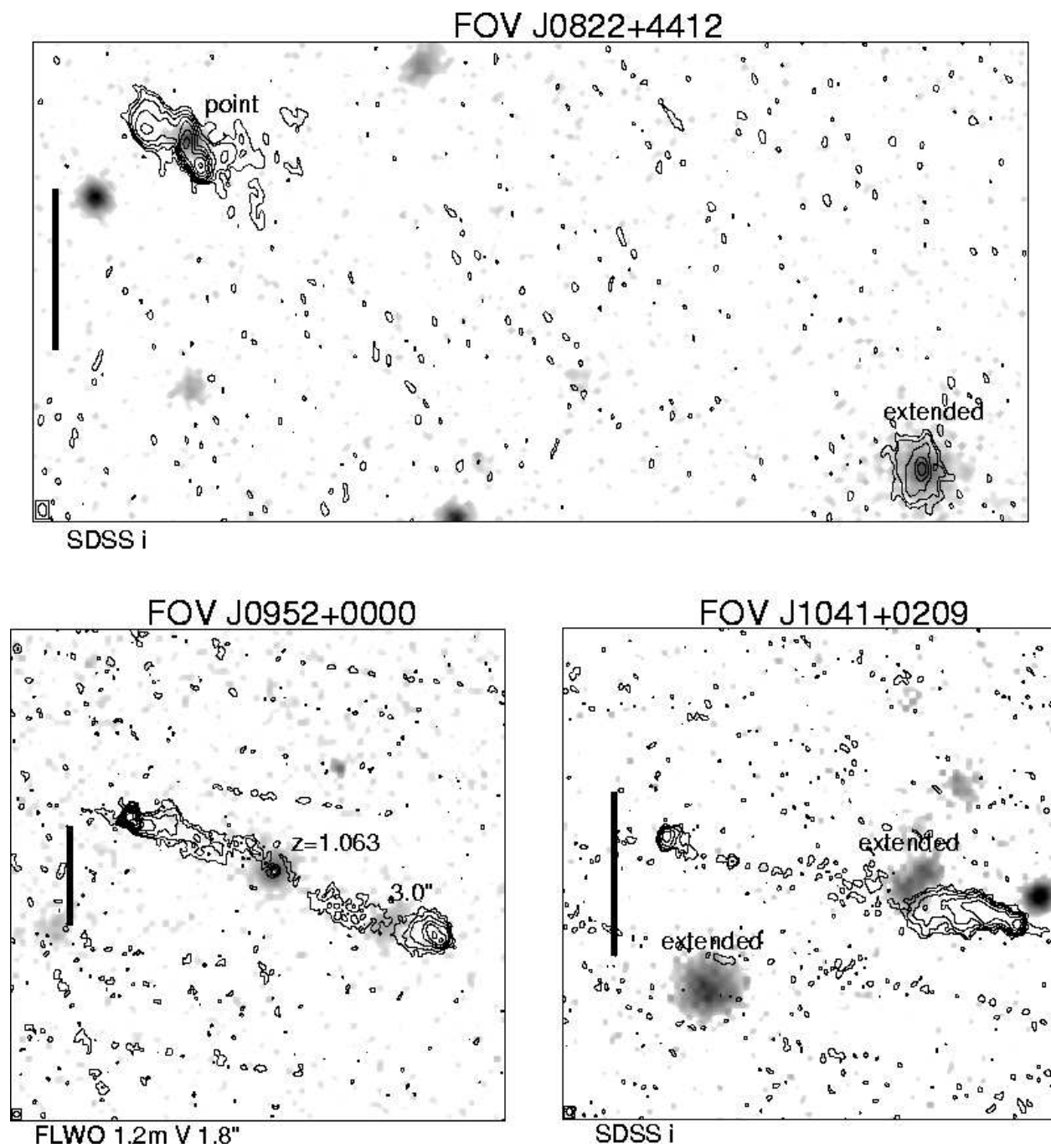


Fig. 1b.— See Figure 1a caption.

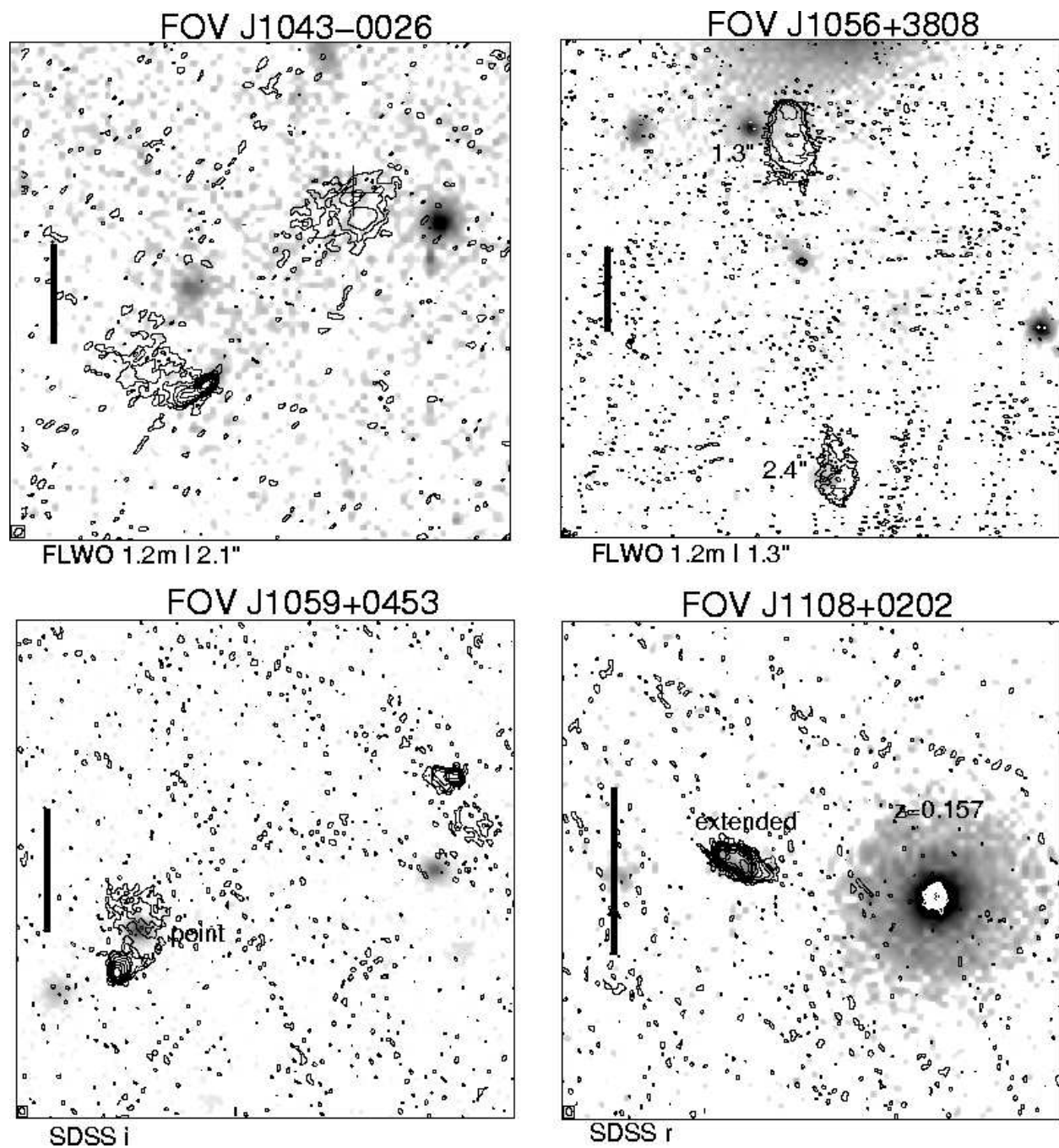


Fig. 1c.— See Figure 1a caption.

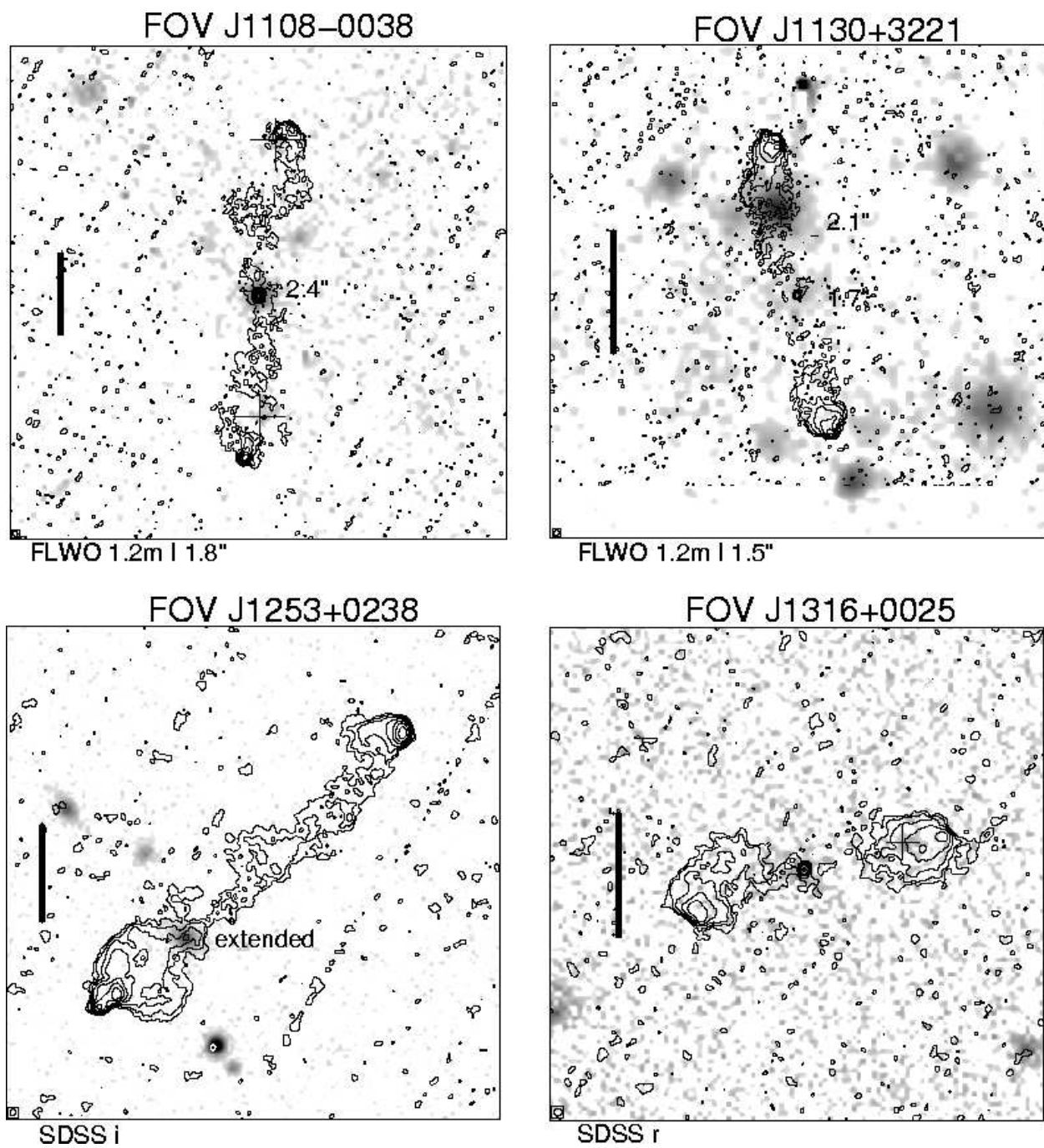


Fig. 1d.— See Figure 1a caption.

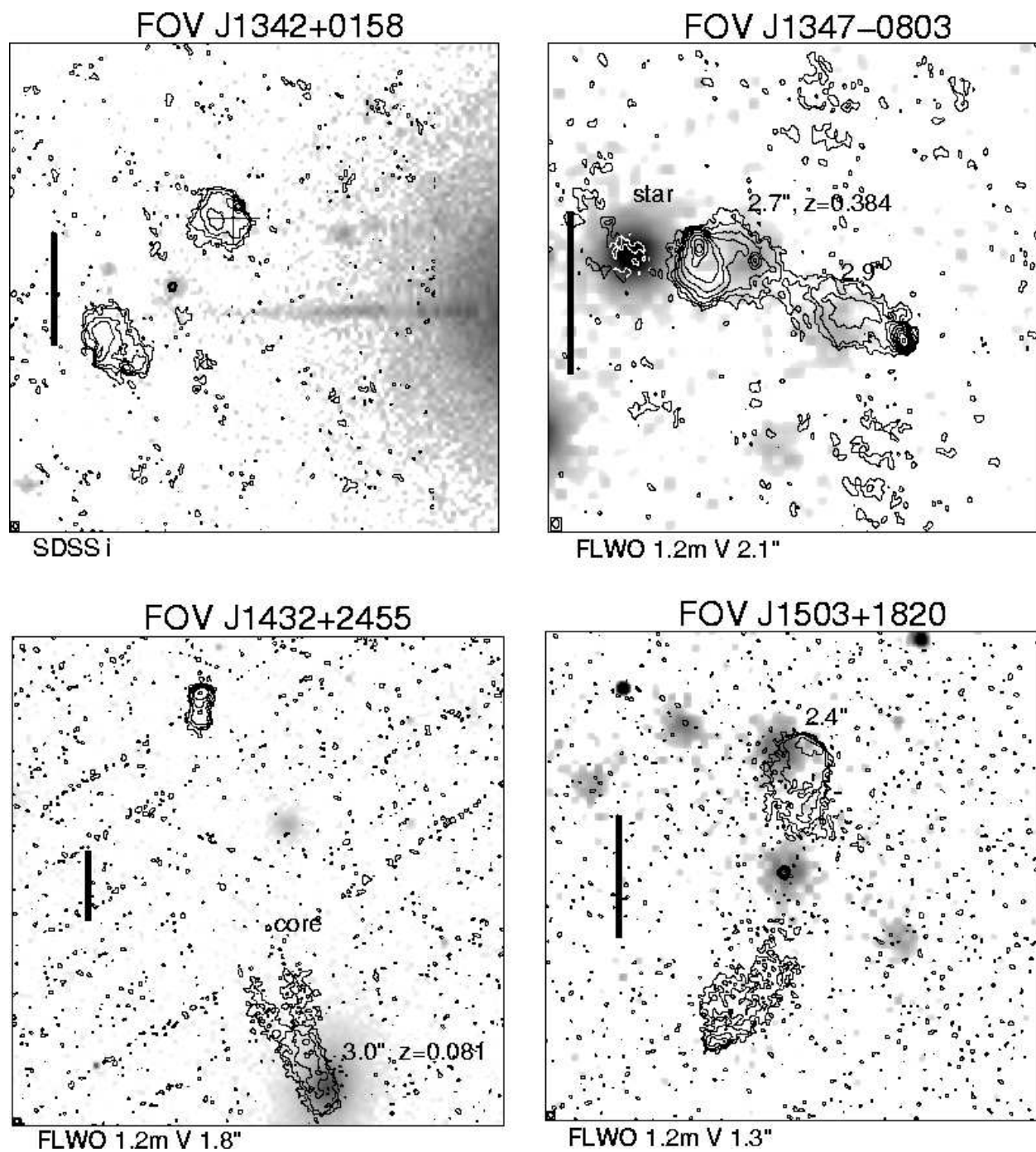


Fig. 1e.— See Figure 1a caption.

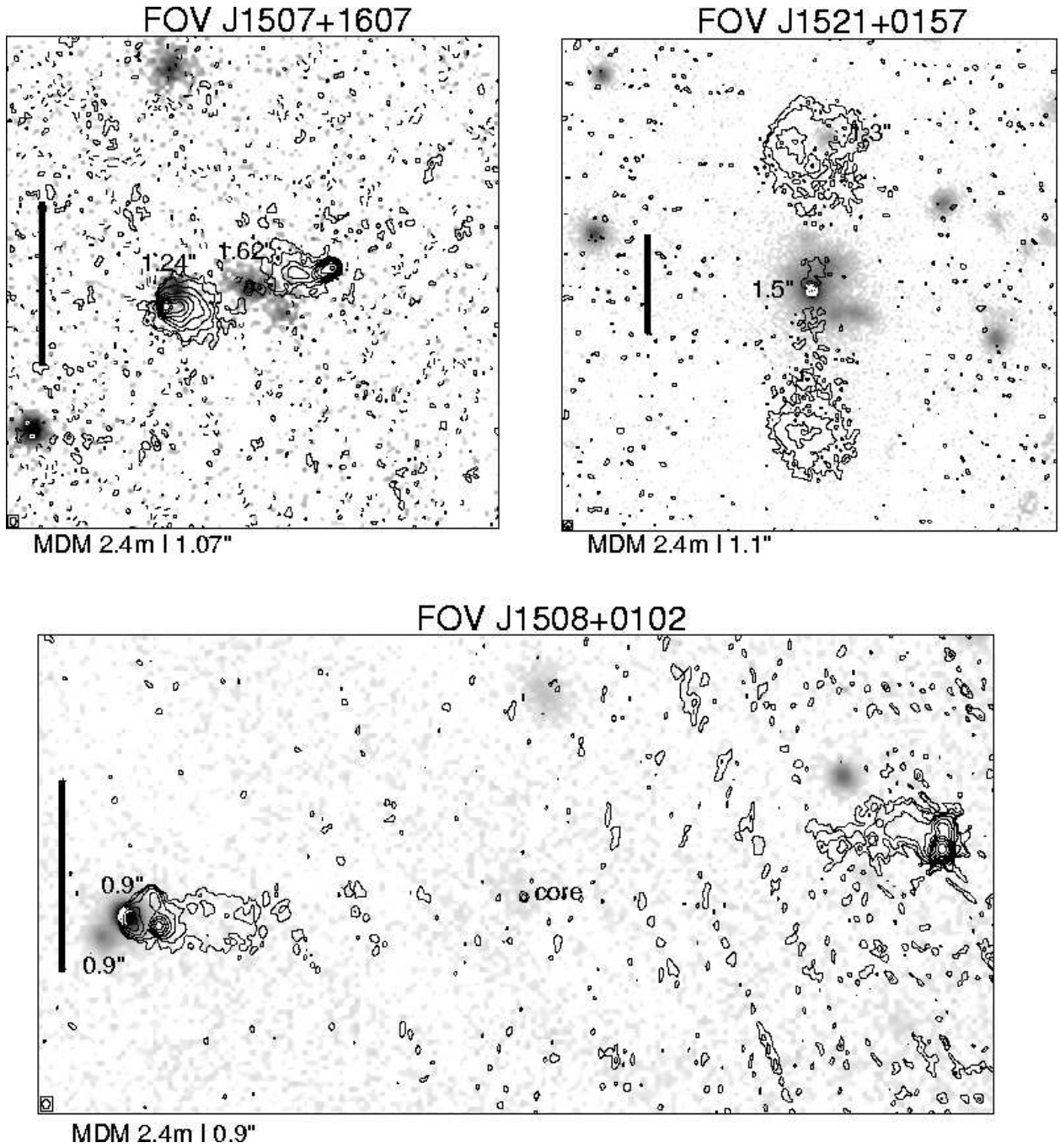


Fig. 1f.— See Figure 1a caption.

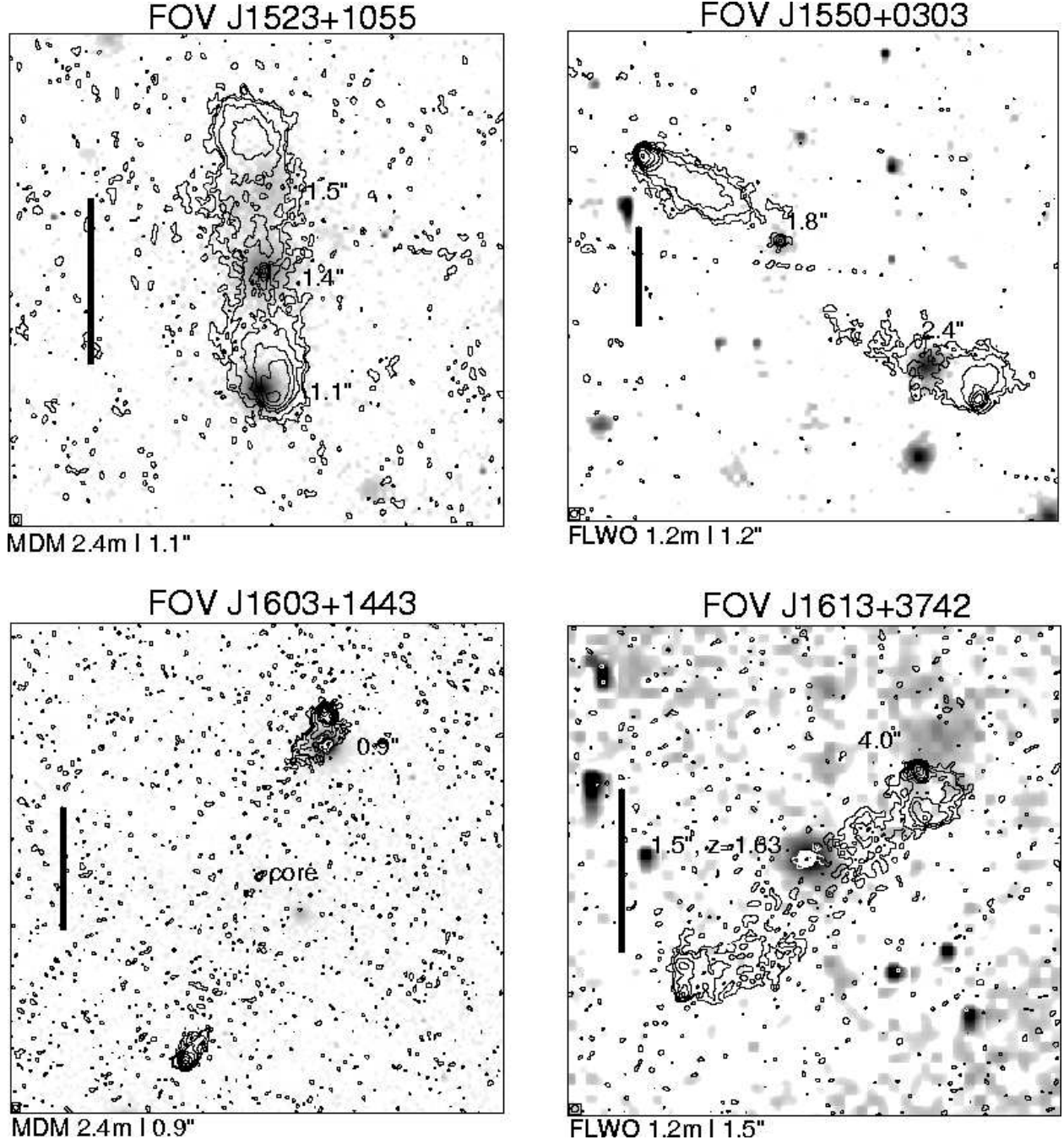


Fig. 1g.— See Figure 1a caption.

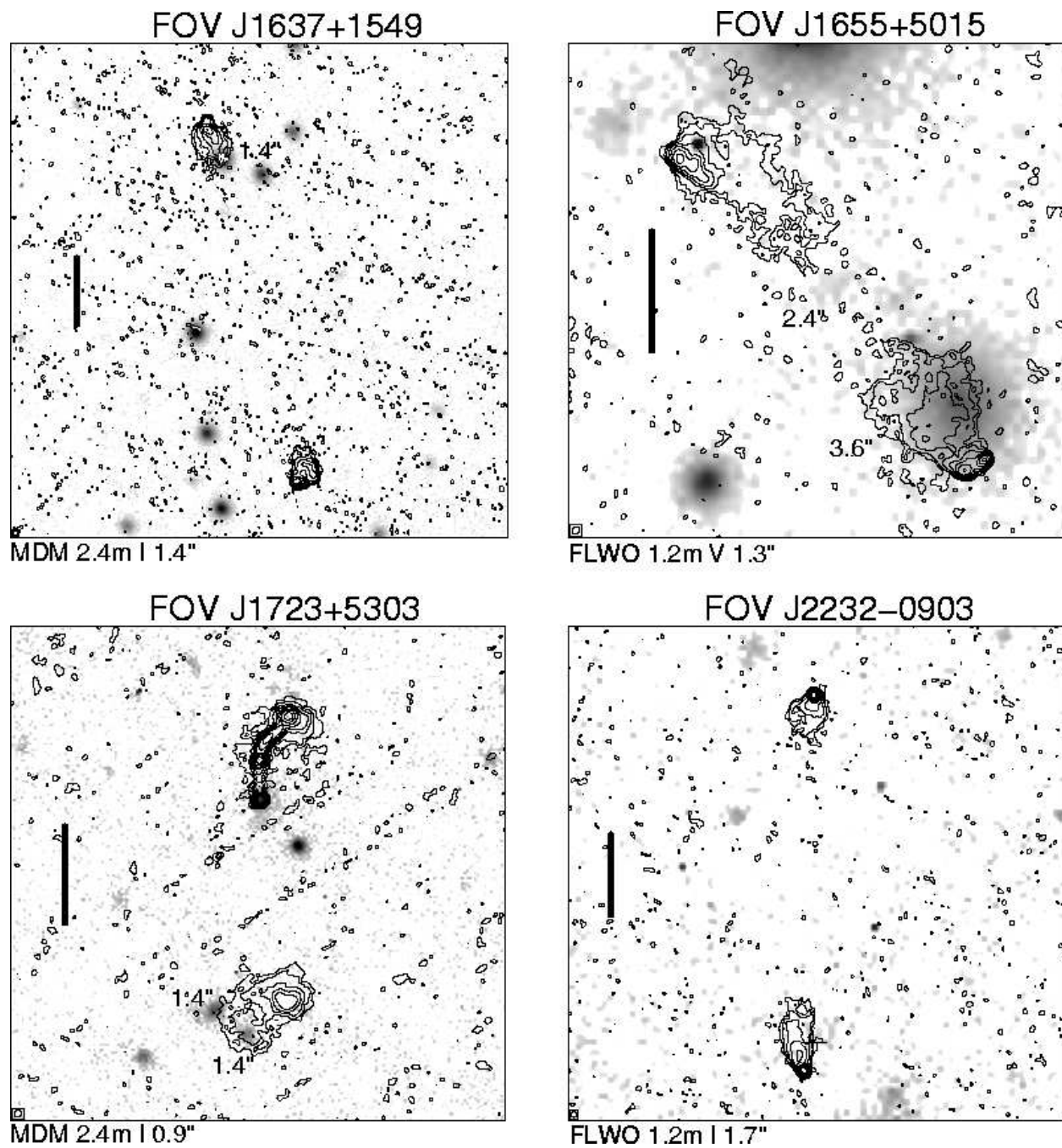


Fig. 1h.— See Figure 1a caption.

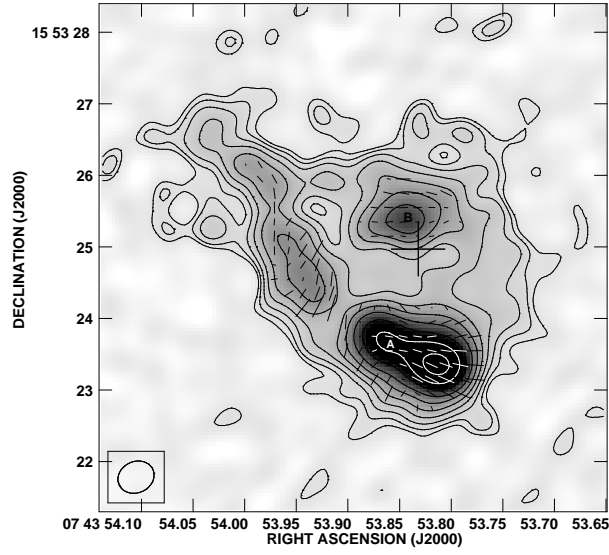


Fig. 2.— VLA 6 cm map of gravitational lens FOV J0743+1553. Intensity contours increase by factors of 1.5 from 1.5 times the off-source rms noise of $50 \mu\text{Jy}$ per beam. The beam is shown in the lower left. The fractional polarization vectors are parallel to the electric field and scaled so that one spacing interval corresponds to 17% polarization per beam. A cross indicates the measured position of the lens galaxy.

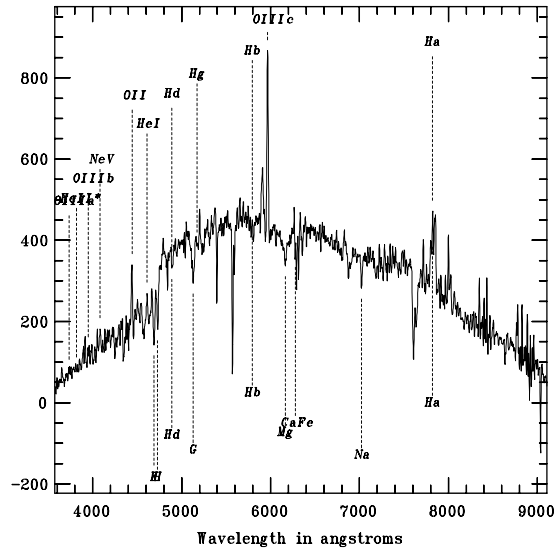


Fig. 3.— Spectrum of lensing galaxy FOV J0743+1553. The data were taken with the BlueChannel instrument on the 6.5 m MMT Observatory, and show a lens redshift 0.1918.

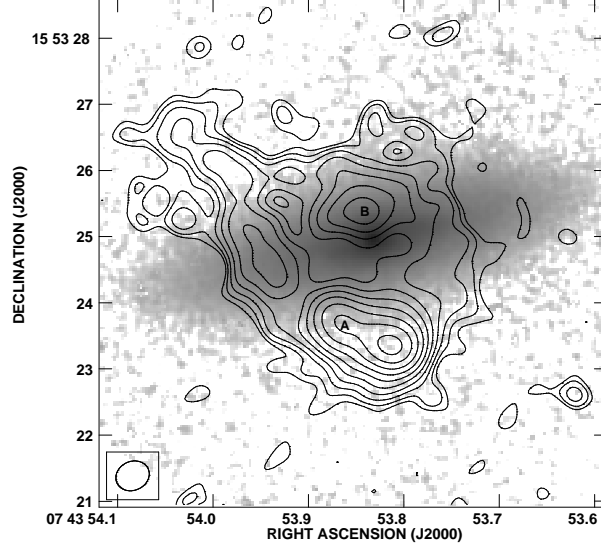


Fig. 4.— Gravitational lens FOV J0743+1553. VLA 6 cm contours are shown as in Figure 2. Hubble Space Telescope NICMOS data in the F160W filter is shown in grey with a logarithmic stretch.

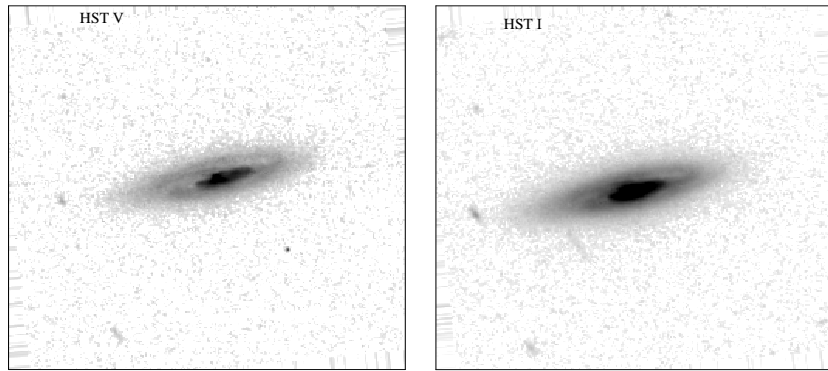


Fig. 5.— Gravitational lens FOV J0743+1553. Hubble Space Telescope ACS data in V (F555W) and I (F814W) is shown with a square-root stretch. Maps are $13'' \times 13''$ with north up and east to the left.

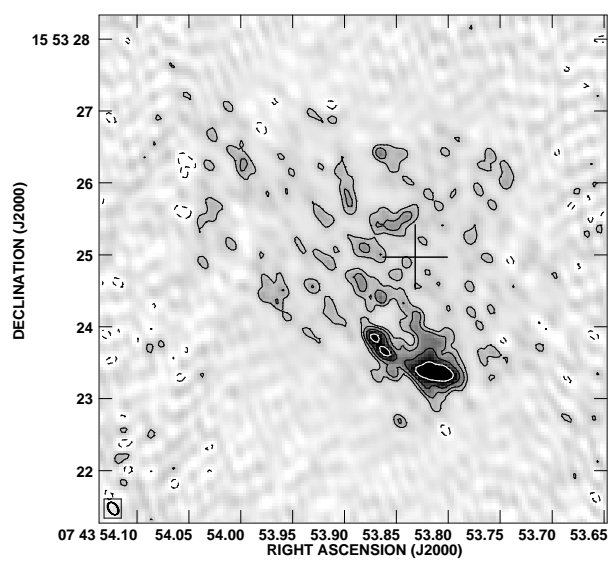


Fig. 6.— MERLIN 18 cm map of FOV J0743+1553. Contours increase by doubling from twice the off-source rms of $72\,\mu\text{Jy/beam}$. A cross indicates the measured center of the lens galaxy.

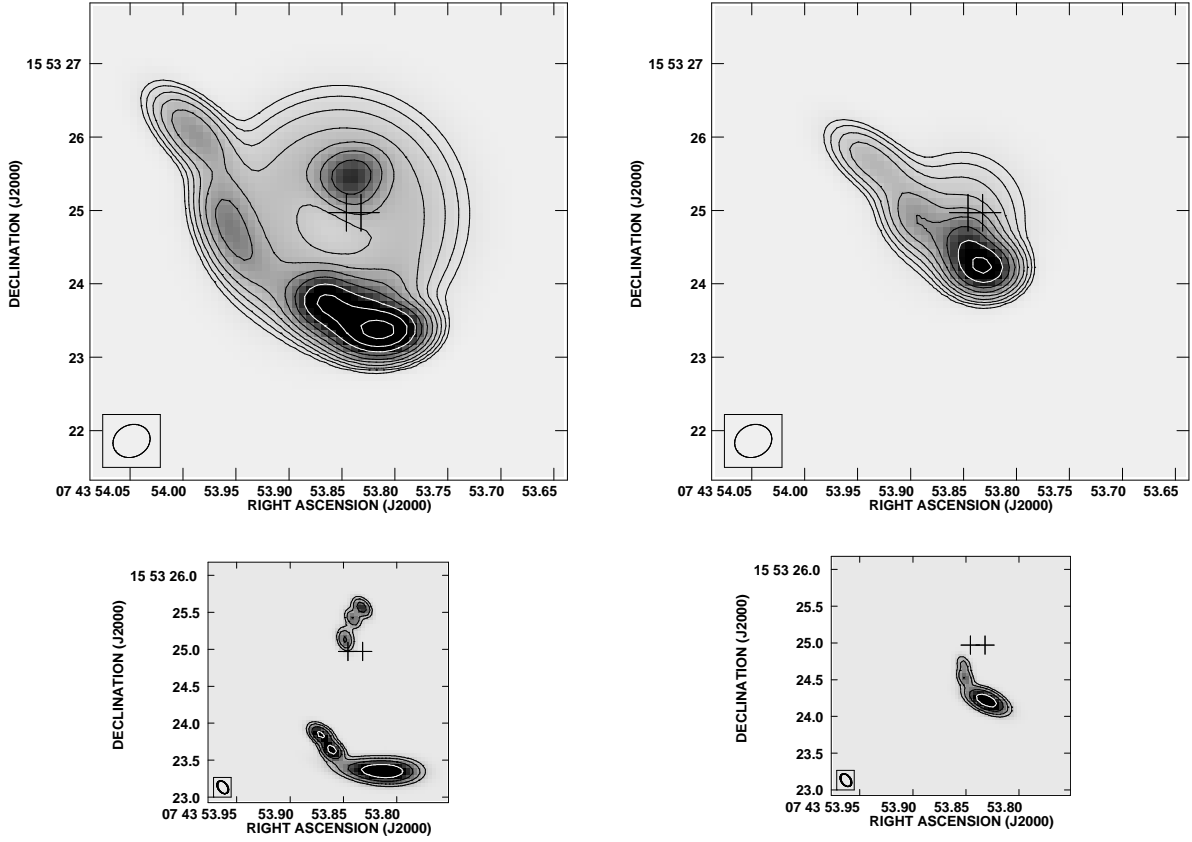


Fig. 7.— Model of FOV J0743+1553. Upper panels at 6 cm, lower panels are 18 cm. On the right, several Gaussian sources represent the unlensed lobe. On the left, a singular isothermal sphere is placed at the location of the eastern cross, reproducing the lensed emission (compare to Figures 2 and 6). The western cross is the observed center of the lens galaxy.

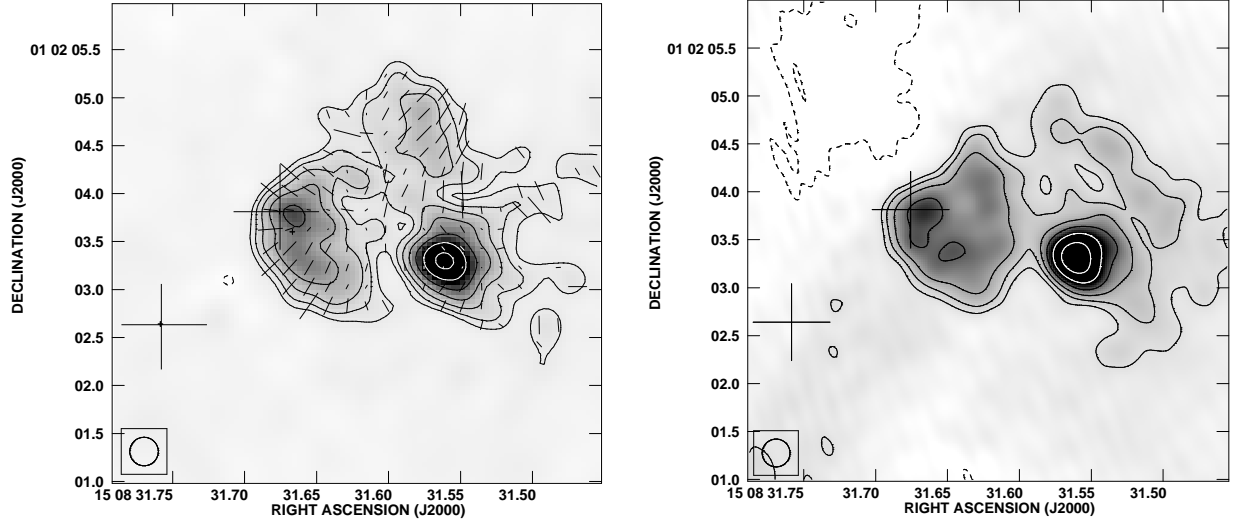


Fig. 8.— Radio maps of the east lobe of FOV J1508+0102. The 6 cm VLA data is shown on the left, and the 18 cm MERLIN data is shown on the right. Both maps have been restored with a $0''.3$ beam to allow direct comparison. Contours in both maps increase by doubling from the off-source rms ($74 \mu\text{Jy/beam}$ in VLA map, $230 \mu\text{Jy/beam}$ in MERLIN map). Crosses mark the location of the two stars in the MDM image. In the 6 cm map, the fractional polarization vectors are parallel to the electric field and scaled so that one spacing interval corresponds to 25% polarization per beam.

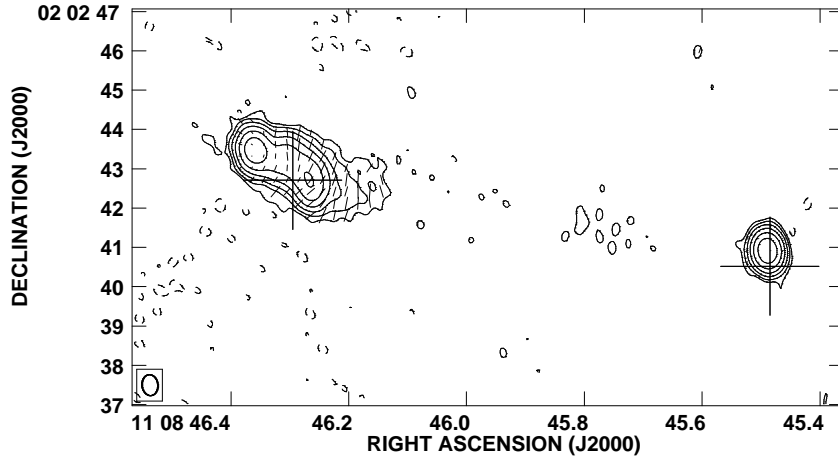


Fig. 9.— VLA 6 cm polarization map of FOV J1108+0202. Contours increase by tripling from three times the off-source rms of $63 \mu\text{Jy}$. The fractional polarization vectors are parallel to the electric field and scaled so that one spacing interval corresponds to 11% polarization per beam.

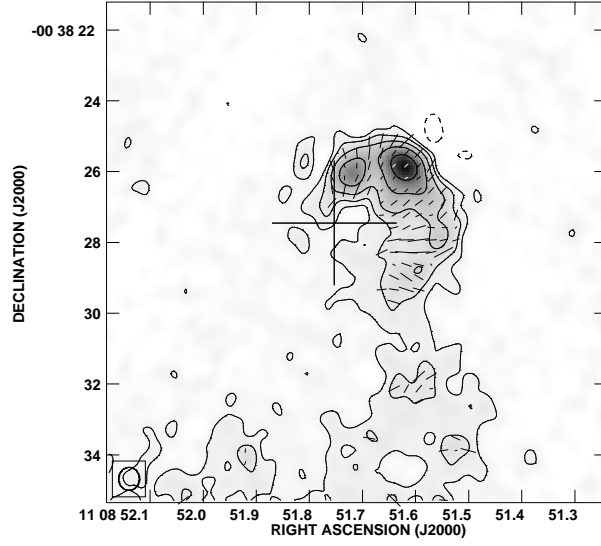


Fig. 10.— VLA 6 cm polarization map of the north lobe of FOV J1108-0038. Contours increase by doubling from twice the off-source rms of $40 \mu\text{Jy}$. The fractional polarization vectors are parallel to the electric field and scaled so that one spacing interval corresponds to 20% polarization per beam.

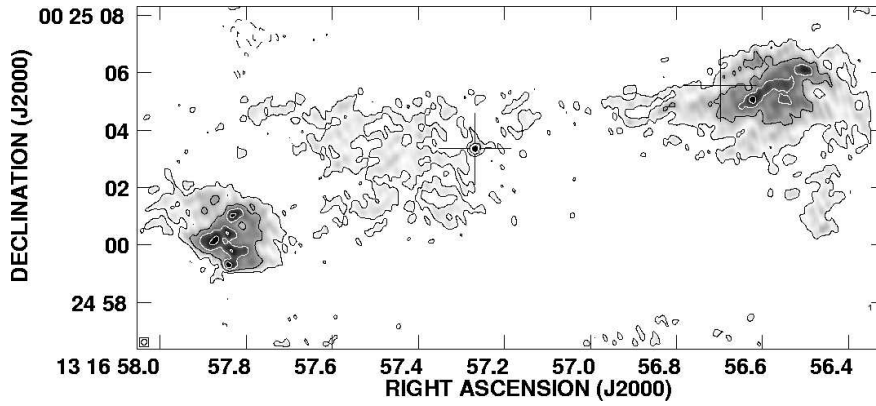


Fig. 11.— MERLIN 18 cm map of FOV J1316+0025. Crosses indicate the location of optical objects. Contours increase linearly from twice the off-source rms of $88 \mu\text{Jy}$. The data were convolved with a circular $0''.2$ beam, shown in the lower right.

Table 1. VLA observations of 92 targets

Name	Coordinates (J2000)	Exp (min)	Wavelength (cm)	Date	Observer
FOV J0040–0146	00:40:57.4 –01:46:18	literature	VLA calibrator, point source
FOV J0040+0125	00:40:13.6 +01:25:46	18	6	2002Mar17	
FOV J0120+0004	01:20:53.9 +00:04:50	12	6	2002Mar17	
FOV J0121+0050	01:21:01.2 +00:51:01	18	6	2002Mar17	
FOV J0143–0118	01:43:16.7 –01:19:01	12	6	2002Mar17	
FOV J0202–0559	02:02:06.9 –05:59:00	18	6	2002Mar17	
FOV J0209–0736	02:09:31.4 –07:36:51	18	6	2002Mar17	
FOV J0233–0203	02:33:28.7 –02:02:56	18	6	2002Mar17	
FOV J0243–0102	02:43:49.4 –01:03:01	18	6	2002Mar17	
FOV J0735+4344	07:35:21.9 +43:44:21	10	6	1994Mar19	C. Carilli
FOV J0743+1553	07:43:54.2 +15:53:33	19	6	2002Mar15	
FOV J0750+2825	07:50:01.8 +28:25:10	12	6	2002Mar17	
FOV J0751+5301	07:51:58.9 +53:01:58	18	6	2002Mar17	
FOV J0804+1721	08:04:19.5 +17:21:33	19	6	2002Mar15	
FOV J0805+1243	08:05:23.4 +12:43:49	19	6	2002Mar15	
FOV J0811+2618	08:11:26.4 +26:18:15	11	4	1995Jul29	K. Blundell
FOV J0815+1741	08:15:34.4 +17:41:56	19	6	2002Mar15	
FOV J0822+4412	08:22:23.8 +44:12:37	19	6	2002Mar15	
FOV J0822+4614	08:22:08.3 +46:14:42	19	6	2002Mar15	
FOV J0912+5320	09:12:03.2 +53:20:28	19	6	2002Mar15	
FOV J0912–0708	09:12:00.5 –07:08:33	19	6	2002Mar15	
FOV J0914+1715	09:14:05.2 +17:15:54	12	6	2002Mar15	
FOV J0935+3633	09:35:30.4 +36:33:08	15	4	1990Jul19	G. Taylor
FOV J0939+0201	09:39:08.2 +02:01:02	19	6	2002Mar15	
FOV J0939+4016	09:39:20.4 +40:16:51	19	6	2002Mar15	
FOV J0945+1428	09:45:27.7 +14:28:17	21	6	2002Mar11	
FOV J0952+0000	09:52:45.7 +00:00:15	21	6	2002Mar11	
FOV J1004+1018	10:04:11.8 +10:18:42	21	6	2002Mar11	
FOV J1004–0715	10:04:23.6 –07:15:12	21	6	2002Mar11	
FOV J1040+2815	10:40:18.7 +28:15:19	19	6	2002Mar15	
FOV J1041+0209	10:41:23.4 +02:09:02	21	6	2002Mar09	
FOV J1043–0026	10:43:09.2 –00:26:29	21	6	2002Mar09	
FOV J1056+3808	10:56:12.4 +38:08:45	19	6	2002Mar15	
FOV J1059+0453	10:59:50.7 +04:53:57	21	6	2002Mar09	
FOV J1102+5550	11:02:26.4 +55:50:02	12	6	2002Mar15	
FOV J1103+5054	11:03:44.5 +50:54:02	19	6	2002Mar15	
FOV J1103–0512	11:03:33.7 –05:12:19	19	6	2002Mar15	
FOV J1106–0052	11:06:31.8 –00:52:52	21	6	2002Mar11	
FOV J1108+0202	11:08:46.0 +02:02:43	21	6	2002Mar11	
FOV J1108–0038	11:08:51.9 –00:38:46	21	6	2002Mar11	
FOV J1112–0025	11:12:31.1 –00:25:34	19	6	2002Mar15	
FOV J1117+1904	11:17:18.7 +19:04:24	12	6	2002Mar15	
FOV J1124+1142	11:24:41.4 +11:42:36	21	6	2002Mar11	
FOV J1129–0703	11:29:12.9 –07:03:20	21	6	2002Mar09	

Table 1—Continued

Name	Coordinates (J2000)	Exp (min)	Wavelength (cm)	Date	Observer
FOV J1130+3221	11:30:33.8 +32:21:38	19	6	2002Mar15	
FOV J1134+0357	11:34:32.2 +03:57:46	21	6	2002Mar11	
FOV J1144+2958	11:44:21.3 +29:58:27	12	6	2002Mar15	
FOV J1145+4420	11:45:38.5 +44:20:22	12	6	2002Mar15	
FOV J1146+1805	11:46:32.1 +18:05:11	19	6	2002Mar15	
FOV J1204–0443	12:04:04.6 –04:43:53	21	6	2002Mar09	
FOV J1209–0257	12:09:06.9 –02:57:46	10	6	1982Jun11	A. Downes
FOV J1214–0100	12:14:48.9 –01:00:17	14	6	2002Mar11	
FOV J1215+0018	12:15:23.1 +00:18:55	12	6	2002Mar15	
FOV J1232–0224	12:32:00.3 –02:24:03	literature	Kronberg et al. 1992 ApJ 387,528
FOV J1253+0238	12:53:03.3 +02:38:25	13	6	2002Mar09	
FOV J1253+1139	12:53:13.4 +11:39:35	14	6	2002Mar11	
FOV J1300+3804	13:00:14.0 +38:04:30	19	6	2002Mar15	
FOV J1304+5324	13:04:44.2 +53:24:16	19	6	2002Mar15	
FOV J1316+0025	13:16:57.3 +00:25:03	21	6	2002Mar11	
FOV J1320+1743	13:20:21.2 +17:43:11	12	6	2002Mar15	
FOV J1331+5426	13:31:29.7 +54:26:30	19	6	2002Mar15	
FOV J1332+0101	13:32:16.5 +01:01:48	11	6	1982Jun12	A. Downes
FOV J1342+0158	13:42:48.4 +01:58:09	11	6	1982Jun12	A. Downes
FOV J1345–0252	13:45:52.2 –02:52:32	11	6	1982Jun12	A. Downes
FOV J1347–0000	13:47:45.1 –00:00:48	13	6	2002Mar09	
FOV J1347–0803	13:47:01.3 –08:03:25	13	6	2002Mar09	
FOV J1357+4807	13:57:30.6 +48:07:42	19	6	2002Mar15	
FOV J1405+2335	14:05:46.1 +23:35:53	19	6	2002Mar15	
FOV J1432+2455	14:32:42.2 +24:55:48	19	6	2002Mar15	
FOV J1444+1131	14:44:50.7 +11:31:56	21	6	2002Mar09	
FOV J1501+0752	15:01:57.5 +07:52:27	21	6	2002Mar11	
FOV J1503+1820	15:03:01.6 +18:20:31	19	6	2002Mar15	
FOV J1507+1607	15:07:09.1 +16:07:17	21	6	2002Mar11	
FOV J1508+0102	15:08:30.3 +01:02:06	21	6	2002Mar09	
FOV J1521+0157	15:21:27.9 +01:57:22	21	6	2002Mar09	
FOV J1523+1055	15:23:57.0 +10:55:43	14	6	2002Mar11	
FOV J1547+2748	15:47:21.0 +27:48:22	19	6	2002Mar15	
FOV J1550+0303	15:50:23.2 +03:03:47	21	6	2002Mar11	
FOV J1603+1443	16:03:05.5 +14:43:32	19	6	2002Mar15	
FOV J1605+0337	16:05:45.1 +03:37:17	19	6	2002Mar15	
FOV J1608+2848	16:08:11.3 +28:49:02	10	6	1981Mar17	R. Sinha
FOV J1613+3742	16:13:51.3 +37:42:58	19	6	2002Mar15	
FOV J1614+0405	16:14:14.5 +04:05:55	14	6	2002Mar11	
FOV J1637+1549	16:37:49.4 +15:49:22	19	6	2002Mar15	
FOV J1655+5015	16:55:22.1 +50:15:15	19	6	2002Mar15	
FOV J1710+4601	17:10:44.1 +46:01:29	literature	3C352
FOV J1714+3001	17:14:10.1 +30:01:24	19	6	2002Mar15	
FOV J1723+5303	17:23:50.0 +53:03:02	19	6	2002Mar15	

Table 1—Continued

Name	Coordinates (J2000)	Exp (min)	Wavelength (cm)	Date	Observer
FOV J1727+5230	17:27:17.7 +52:30:33	12	6	2002Mar15	
FOV J2232–0903	22:32:31.8 –09:03:37	18	6	2002Mar17	
FOV J2245–0204	22:45:43.4 –02:04:46	18	6	2002Mar17	
FOV J2333–1032	23:33:43.9 –10:32:20	18	6	2002Mar17	

Note. — Coordinates are of the center of the map (if shown in Figure 1), the radio core (if present and unambiguous), or the midpoint of the FIRST components (all others).

Table 2. Optical data on 32 Targets

Name	Coordinates (J2000)	CCD Observations								
		Catalog Lens Magnitudes			Telescope, Band	Seeing (arcsec)	Lens FWHM (arcsec)	Core detected?		
								VLA	CCD	
FOV J0121+0050	01 21 01.47 +00 50 47.6	APM POSS	R=19.1	B=21.9	Magellan, i'	0.66	0.90	yes	yes	
FOV J0243-0102	02 43 49.12 -01 02 53.4	SDSS EDR	r=22.6	g=23.5	Magellan, i'	1.8	2.2	no	no	
FOV J0743+1553	07 43 53.84 +15 53 24.9	APM POSS	R=18.6	B>21.5	FLWO 1.2m, I	1.7	2.3	yes	no	
FOV J0822+4412 W	08 22 21.56 +44 12 24.2	APM POSS	R=19.2	B>21.5	SDSS DR1, i	...	extended	yes	yes	
FOV J0939+4016	09 39 20.63 +40 17 02.8	APM POSS	R=19.1	B=21.7	FLWO 1.2m, I	1.6	1.8	yes	no	
FOV J0952+0000	09 52 44.81 +00 00 10.0	APM UKST	R=19.6	B=20.7	FLWO 1.2m, I	1.8	3.0	yes	yes	
FOV J1041+0209	10 41 22.90 +02 09 02.2	APM UKST	R=19.3	B=20.4	SDSS DR1, i	...	extended	yes?	no	
FOV J1043-0026	10 43 08.58 -00 26 19.0	SDSS EDR	r=23.0	g=23.4	FLWO 1.2m, I	2.1	detected?	yes	?	
FOV J1056+3808	10 56 12.24 +38 08 21.5	APM POSS	R>20	B=22.1	FLWO 1.2m, I	1.3	2.4	yes	yes	
FOV J1059+0453	10 59 51.38 +04 53 52.0	APM POSS	R=17.9	B>21.5	SDSS DR1, i	...	point	no	no	
FOV J1108+0202	11 08 46.28 +02 02 42.7	APM UKST	R>21	B=21.0	SDSS DR1, r	...	extended	yes	yes	
FOV J1108-0038 N	11 08 51.75 -00 38 27.5	SDSS EDR	r=22.5	g=23.9	FLWO 1.2m, I	1.8	detected?	yes	yes	
FOV J1108-0038 S	11 08 51.86 -00 39 01.4	SDSS EDR	r=21.4	g=25.0			detected			
FOV J1130+3221	11 30 33.94 +32 21 44.9	APM POSS	R=18.6	B>20.6	FLWO 1.2m, I	1.5	2.1	yes	yes	
FOV J1253+0238	12 53 03.72 +02 38 18.3	APM POSS	R=18.3	B=21.2	SDSS DR1, i	...	extended	yes	yes	
FOV J1316+0025	13 16 56.70 +00 25 05.6	SDSS EDR	r=22.2	g=22.4	SDSS DR1, i	...	detected	yes	yes	
FOV J1342+0158	13 42 48.00 +01 58 15.5	APM UKST	R>21	B=21.7	SDSS DR1, i	...	not detected	yes	yes	
FOV J1347-0803	13 47 01.47 -08 03 23.3	APM UKST	R=19.9	B=21.6	FLWO 1.2m, I	2.1	2.9	yes	yes	
FOV J1432+2455	14 32 41.46 +24 55 18.2	APM POSS	R=15.1	B=16.9	FLWO 1.2m, I	1.8	3.0	yes	no	
FOV J1503+1820	15 03 01.67 +18 20 41.4	APM POSS	R=19.0	B=20.6	FLWO 1.2m, I	1.3	2.4	yes	yes	
FOV J1507+1607	15 07 09.42 +16 07 16.3	DPOSS	i=20.9	g=20.9	MDM 2.4m, I	1.07	1.24	yes	yes	
FOV J1508+0102	15 08 31.68 +01 02 03.8	APM UKST	R=19.0	B=21.0	MDM 2.4m, I	0.9	0.9	yes	?	
FOV J1521+0157	15 21 27.79 +01 57 36.8	APM UKST	R>21	B=23.6	MDM 2.4m, I	1.1	1.3	yes	yes	
FOV J1523+1055 N	15 23 56.96 +10 55 48.5	APM POSS	R>20	B=21.2	MDM 2.4m, I	1.1	1.5	yes	yes	
FOV J1523+1055 S	15 23 56.99 +10 55 36.0	DPOSS	r=19.8	g=21.5			1.1			
FOV J1550+0303	15 50 22.41 +03 03 37.7	APM POSS	R=19.4	B>21.5	FLWO 1.2m, I	1.2	2.4	yes	yes	
FOV J1603+1443	16 03 05.11 +14 43 42.3	APM POSS	R=17.5	B=20.6	MDM 2.4m, I	0.9	0.9	yes	no	
FOV J1613+3742	16 13 50.7 +37 43 05.8	APM POSS	R>20	B=21.2	FLWO 1.2m, I	1.5	4.0	yes	yes	
FOV J1637+1549	16 37 49.76 +15 49 41.0	APM POSS	R=18.5	B>21.5	MDM 2.4m, I	1.4	1.4	no	no	
FOV J1655+5015	16 55 20.91 +50 15 05.9	APM POSS	R=17.5	B=18.9	FLWO 1.2m, I	1.3	3.6	no	?	
FOV J1723+5303	17 23 50.14 +53 02 45.5	SDSS EDR	r=22.0	g=25.1	MDM 2.4m, I	0.9	1.4	yes	yes	
FOV J2232-0903	22 32 31.82 -09 03 57.7	APM UKST	R>21	B=22.3	FLWO 1.2m, I	1.7	detected?	no	no	

Table 2—Continued

Name	Coordinates (J2000)	Catalog Lens Magnitudes	CCD Observations			Core detected?	
			Telescope, Band	Seeing (arcsec)	Lens FWHM (arcsec)	VLA	CCD

Note. — Objects FOV J1108–0038 and FOV J1523+1055 each have two potential lens galaxies. Objects FOV J1507+1607 and FOV J1523+1055 were selected based on an APM catalog entry, but some components in the image didn’t appear in the APM catalog, so DPOSS data were used (DPOSS is the Digitized Palomar Observatory Sky Survey, <http://taltos.pha.jhu.edu/~rrg/science/dposs>).

Table 3. Status of 32 Targets

Name	Optical status	Radio status
FOV J0121+0050	aligned galaxy	lobe, $z = 0.237$
FOV J0243–0102	aligned galaxy	lobe
FOV J0743+1553	aligned galaxy, $z = 0.1918$	lobe with possible lensed features
FOV J0822+4412 W	starburst galaxy?	starburst galaxy?
FOV J0939+4016	aligned galaxy, $z = 0.186$	lobe
FOV J0952+0000	aligned galaxy	lobe, $z = 1.063$
FOV J1041+0209	not aligned	lobe
FOV J1043–0026	extent not measured	lobe
FOV J1056+3808	aligned galaxy	lobe
FOV J1059+0453	star	lobe
FOV J1108+0202	aligned galaxy	lobe, $z = 0.157$
FOV J1108–0038 N	extent not measured	lobe
FOV J1108–0038 S	extent not measured	lobe
FOV J1130+3221	aligned galaxy	lobe
FOV J1253+0238	aligned galaxy	core
FOV J1316+0025	extent not measured	lobe
FOV J1342+0158	spurious catalog entry	lobe
FOV J1347–0803	aligned galaxy	lobe, $z = 0.384$
FOV J1432+2455	aligned galaxy, $z = 0.081$	lobe
FOV J1503+1820	aligned galaxy	lobe
FOV J1507+1607	aligned galaxy	lobe
FOV J1508+0102	double star	lobe with possible lensed features
FOV J1521+0157	aligned galaxy	lobe
FOV J1523+1055 N	aligned galaxy	lobe
FOV J1523+1055 S	star	lobe
FOV J1550+0303	aligned galaxy	lobe
FOV J1603+1443	star	lobe
FOV J1613+3742	not aligned	lobe with possible lensed features, $z = 1.63$
FOV J1637+1549	star? (extent $\leq 1''.4$)	lobe
FOV J1655+5015	aligned galaxy	lobe
FOV J1723+5303	aligned galaxy	lobe
FOV J2232–0903	not aligned	lobe

Table 4. Two components of the light distribution of spiral galaxy FOV J0743+1553

DeVaucouleurs (bulge)		Exponential Disk	
H mag	17.44 ± 0.05	H mag	16.20 ± 0.04
R_{eff}	$0.27 \pm 0.02''$	scale	$0.84 \pm 0.02''$
b/a	0.71 ± 0.02	b/a	0.25 ± 0.01
PA	$-74. \pm 2.^\circ$	PA	$-77.3 \pm 0.1^\circ$

Note. — The errors were calculated from the dispersion of fits using the various sub-exposures and by using 12 different PSF stars.